Helsinki University of Technology
Department of Electrical and Communications Engineering
Optoelectronics Laboratory
Espoo, Finland 2004

FIBER AMPLIFIERS, DIRECTLY MODULATED TRANSMITTERS AND A RING NETWORK STRUCTURE FOR OPTICAL COMMUNICATIONS

Simo Tammela

Thesis for the degree of Doctor of Science in Technology to be presented with due permission for public examination and debate in Auditorium B at Helsinki University of Technology, Espoo, Finland, on the 21st of January, 2004, at 12 o'clock noon.

Helsinki University of Technology
Department of Electrical and Communications Engineering
Optoelectronics Laboratory

Distribution:
Helsinki University of Technology
Department of Electrical and Communications Engineering
Optoelectronics Laboratory
P.O. Box 3500
FIN-02015 HUT, Finland
FINLAND

ISBN 951-22-6902-3
Otamedia Oy

Espoo 2004

ABSTRACT

The three technologies that are considered the key elements in building a metropolitan area optical network are studied in this thesis. They are optical amplification, high-speed low cost transmitters and ring network structures. These studies concentrate on cost reduction of these three technologies thus enabling the use of optical networks in small customer base metropolitan areas.

The research on optical amplification concentrated first on the solution doping process, at present the most used method for producing erbium doped fiber. It was found that separationing the soot growth and the sintering improved the uniformity of the porous layer. This made the homogeneity of the doping concentration in the fiber core better. The effects of index profile variations that arise from the non-ideal solution doping process were also simulated. In the search for a better doping method a new nanoparticle glass-forming process, the direct nanoparticle deposition, was developed. In this process the doping is done simultaneously with glass formation. Utilizing this new process it was possible to improve the uniformity of the doping resulting in higher usable doping levels and shorter erbium doped fiber lengths in the amplifiers. There were fewer limitations in the amplifier caused by optical non-linearities and polarization mode dispersion since shorter fiber lengths were needed.

The double cladding fiber, which avoids the costly coupling of the pump laser into a single mode waveguide, was also studied. This pumping scheme was found to improve the inversion uniformity in the erbium doped fiber core thereby enhancing the power conversion efficiency for the long wavelength band amplifier.

In characterizing the erbium doped fiber amplifier the gain and noise figure was measured with a temporal filter setup. It was made of simple, low cost components but yielded accurate measurements since the noise originating from the amplified spontaneous emission was measured at the signal wavelength. In the study of fiber amplifier controlling schemes the input power of the fiber amplifier was successfully used to regulate the pump laser. This feed-forward control scheme provides a simple, low cost control and managment system for the erbium doped fiber amplifier in metropolitan area network applications that require flexible adding and dropping of wavelength channels.

The transmitter research focused on the DFB laser due to its simplicity and low cost structure. A solid state Fabry-Perot etalon made from double polished silicon chip was used as a frequency discriminator in the chirp analyser developed for the DFB lasers. This wavelength discriminator did not require repeated calibration or active stabilisation and was controled electrically enabling automatic measurements. The silicon Fabry-Perot etalon was also used for simultaneous spectral filtering and wavelength control of the laser. The usable dispersion limited transmission length was increased when the filter was used in conjunction with the directly modulated distributed feedback laser transmitter.

The combination of spatial multiplexing and dense wavelength division multiplexing in ring topology was investigated in the course of the research on the ring network as the feeder part of the metropolitan network. A new way to organize different wavelengths and fibers was developed. This ring network structure was simulated and an experimental ring network built. The results of the studies demonstrated that the same limitations effecting uni-directional ring structures also are the main limitations on the scalability of the spatial and wavelength division multiplexed ring networks based on bi-directional transmission when the node spacing is short. The developed ring network structure demonstrated major cost reductions when compared with the heavy use of wavelength division multiplexing. The node structure was also greatly simplified resulting in less need for different

wavelength transmitters in each node. Furthermore the node generated only minor losses for the passing signals thus reducing the need for optical amplification.

PREFACE

This work was carried out mainly at VTT-Microelectronics (Semiconductor laboratory until 1993) 1984-2000 and continued at Liekki Oy, 2000-2003. Several other companies have contributed to this work. The most signifigant being Nokia Oy, NK-Cables, and Teleste Oy. The author has also had the privilege to take part in the hard but rewarding process of development of commercial products and production systems within these companies.

Acknowledgements

It is self-evident that this kind of work requires more than one person's effort. I have had the fortune to work under the inspiring supervision of Prof. Matti Leppihalme, the leader of the Photonics group, who has created the innovative atmosphere needed for this work. I also express my thanks to Prof. Jouni Heleskivi, the former leader of the laboratory, for enabling this long-term project. I owe huge thanks also to Liekki Oy, especially Markku Rajala and Marjatta Kuusi as well as to the Academy of Finland for making possible to finalise this work.

I'm in an enormous debt to my colleagues at VTT. I want to name a few among the many people: Mr. Ingmar Stuns who made the impossible gadgets that enabled the realisation of the inventions. Mr. Jukka Pihlainen who's expertise in electronics was essential. Mrs Päivi Heimala who's processing know-how in realising optics on silicon enabled the fabrication of Fabry-Perot filters. Mr. Mikko Söderlund who made the tools for the EDFA simulations. Mr. Kalle Ylä-Jarkko who became acquainted with the metropolitan area optical networks. Mr. Joona Koponen and Mr. Ari Hokkanen who have realised among other things a huge number of measurement set-ups used in the studies presented here.

Due to the long time period many of my close colleagues have changed employers. They have continued to participate in this work in many ways after leaving VTT and have thus strengthened the vital bindings between the research community and the industry. I want to give my special thanks to Dr. Pauli Kiiveri of Liekki Oy and Dr. Ari Tervonen of Nokia Research Center. Both have been my long-term co-workers. Most of the work related to erbium doped fiber and EDFAs has been carried out with Pauli, and Ari has been a crucial partner in the development of the ring network. I thank also Mrs Arja Heinämäki who participated in the creation of a commercial product from EDFA and Dr. Jaakko Aarnio who provided deeper understanding of the telecommunication networks. I'd like to express my gratitude also to Dr. Pekka Pöyhönen, Dr. Seppo Honkanen, Mr. Hans von Bagh and Mrs. Ann-Mari Peder-Gothoni for the good co-operation in the course of this work.

The personnel of Liekki, who have enabled the use of the new direct nanoparticle deposition technology for producing erbium doped fiber have contributed enormously to the work presented in publication III. I thank you for this and for the positive attitude, which made it possible to go through all the problems encountered.

I want to acknowledge the Fabry-Perot working group, Dr. Hanne Ludvigsen, Prof. Matti Kaivola, Dr. Timo Kajava and especially the operating muscle of the group, Dr. Tapio Niemi. The help from Ms. Maria Uusimaa in the spectral filtering is also acknowledged. The Silicon Fabry-Perot project has showed the usefulness of co-operation between applied and basic research.

I express also my gratitude for the support from Mr. Jukka Mikkola, Ms. Päivi Männistö, Mr. Ari Salomaa (currently at Liekki Oy) and Mr. Per Öhman from Nokia Oy in the development work on the EDFA.

Finally I thank my wife, Erika Hindsberg and my son Juhani Tammela for understanding and encouraging me during the period of heavy writing of these theses.

LIST OF PUBLICATIONS

I S. Tammela, X. Zahn, P. Kiiveri, Comparison of gain dependence of different Er-doped fibre structures, First publication: Proceedings of the Conference Fiber Laser Sources and Amplifiers II, **1373**, 103-110, 1990; Reprinted: SPIE Milestone Series, **MS 37**, 189 - 195, 1992.

II P. Kiiveri, and S. Tammela, Design and Fabrication of Er-doped Fibers for Optical Amplifiers, Optical Engineering, **39** (7), 1943-1950, 2000.

III S. Tammela, M. Hotoleanu, P. Kiiveri, H. Valkonen, S. Sarkilahti, K. Janka, Very short Er-doped silica glass fiber for L-band amplifiers, Technical Digest of the Optical Fiber Communication Conference (OFC), **1,** 376-377, 2003.

IV M. Söderlund, S. Tammela, P. Pöyhönen, M. Leppihalme and N. Peyghambarian, Amplified Spontaneus Emission in Cladding-Pumped L-band Erbium Fiber Amplifiers, IEEE Photonics Technology Letters, **13**(1), 22-24, 2001.

V P. Kiiveri and S. Tammela, Spectral gain and noise measurement system for fibre amplifiers, Optical Engineering, **34**(9), 2592 - 2596, 1995.

VI M. Söderlund and S. Tammela, Performance of a practical gain-controlling approach for erbium-doped fiber amplifier", Proceedings of the Conference Rare-Earth-Doped Materials and Devices IV, SPIE, **3942**, 210-216, 2000.

VII S. Tammela, H. Ludvigsen, T. Kajava, and M. Kaivola, Time-resolved frequency chirp measurement using a silicon-wafer etalon, IEEE Photonics Technology Letters **9**(4), 1041 - 1135, 1997.

VIII T. Niemi, S. Tammela, T. Kajava, M. Kaivola, and H. Ludvigsen, Temperature-tuneable silicon-wafer etalon for frequency chirp measurements, Microwave and Optical Technology Letters, **20**(3), 190-192, (1999).

IX T. Niemi, M. Uusimaa, H. Ludvigsen, S. Tammela, P. Heimala, T. Kajava, and M. Kaivola, Simultaneous spectral filtering and wavelength monitoring of a DWDM transmitter using a tuneable Fabry-Perot filter, Technical Digest of the Optical Fiber Communication Conference (OFC), **Wednesday**, 28-30, 2000.

X S. Tammela, J. Aarnio, and A. Tervonen, Survivable WDM/SDM ring for metropolitan networks, Proceedings of the Conference on All-Optical Networking: Architecture, Control, and Management Issues, SPIE, **3531**, 448-454, 1998.

XI K. Ylä-Jarkko, S. Tammela, and A. Tervonen, Bidirectional WDM multifiber ring network with Shared-pump EDFA's, Proceedings of the 25th European Conference on Optical Communication (ECOC), **2**, 46-47, 1999.

XII K. Ylä-Jarkko, M. Leppihalme, S. Tammela, T. Niemi, and A. Tervonen, Scalability of a Metropolitan Biderectional Multifiber WDM-Ring Network, Photonic Network Communications, **3**(4), 349-362, 2001.

DESCRIPTION OF THE PUBLICATIONS

Publication I presents the simulation results of different erbium doped fiber structures. It studies theoretically the effects of the non-ideal refractive index profile. The non-ideal index profiles are due to the processing induced effects such as index dip and dopant diffusion.

Publication II describes how the solution doping process of erbium doped fiber can be improved by using reverse growing direction in modified chemical deposition system. It also provides a recipe how erbium doped fibers are produced using solution-doping method.

Publication III shows that it is possible to produce an efficient and short erbium doped fiber for the long wavelength band amplifier using direct nanoparticle deposition technology. The high erbium concentration and short erbium doped fiber in the long wavelength band fiber amplifier decrease the four-wave mixing gain of the fiber amplifier significantly.

In publication IV the use of double cladding erbium doped fiber in long wavelength band erbium doped fiber amplifier is modelled and the impact of the pump cladding area is studied in detail.

Publication V presents the possibility of using temporal filtering techniques to remove the signal from the noise spectrum of the erbium doped fiber amplifier. The outcome of this is an accurate method for noise figure measurement.

Publication VI studies the feed-forward method of controling the erbium doped fiber amplifier gain using direct pump power control.

Publication VII describes a new way to realise a simple and accurate system for measuring the distributed feedback lasers chirp. The measurement is based on the use of solid silicon wafer as Fabry-Perot etalon.

Publication VIII presents a chirp analyser based on a temperature tunable solid silicon chip as Fabry-Perot etalon. An electrical heater integrated on the chip enables automation of the measurement.

Publication IX describes a temperature tunable silicon based Fabry-Perot filter, which simultaneously improves the chirp effect in a distributed feedback laser by spectral filtering and monitors the wavelength with superior accuracy.

Publication X presents a new optical ring network structure combining the benefits of bi-directional transmission, spatial multiplexing and wavelength division multiplexing.

Publication XI presents the experimentally measured characteristics of the test-bed for the ring network introduced in publication X. Also the shared pump scheme is introduced into this network structure.

Publication XII studies the scalability of the ring network introduced in the publication XI and the publication X.

THE AUTHOR'S CONTRIBUTION

The author was involved in generating the ideas presented in the publications and is one of the inventors of the discoveries presented in publications I, II, III, V, VI, VII, VIII, IX, X, and XI. The author has contributed to the design and fabrication of the fibers and components presented in publications II, III, VII, VIII, IX, XI and XII. The author is also responsible for the design and realisation of the measurement systems presented in publications IV, VII, VIII, and IX. The design and construction of the test beds as well as the measurements in publications XI, XII has partly been done by the author. The author has also contributed to the design and realisation of the simulation software presented in publications I and VI. Publications I, VII, X, were written primarily by the author. A signifigant part of publications II, III, V, XI, is credited to the author and the author has also contributed to the writing of publications IV, VI, VIII, IX, XII.

CONTENTS

ABBREVIATIONS AND ACRONYMS

ASE	Amplified spontaneous emission
ATM	Asynchronous transfer mode
CATV	Community antenna television
C-band	Conventional wavelength band
CNR	Carrier to noise ratio
DC	Double cladding
DFB	Distributed feedback
DND	Direct nanoparticle deposition
DWDM	Dense wavelength division multiplexing
ECOC	European Conference on Optical Communication
EDF	Erbium doped fiber
EDFA	Erbium doped fiber amplifier
F-P	Fabry-Perot
FSR	Free spectral range
FWM	Four-wave mixing
HF	High frequency
ICC	IEEE International Conference on Communications
IP	Internet protocol
L-band	Long wavelength band
MAN	Metro area network
MCVD	Modified chemical vapour deposition
M-Z	Mach-Zehnder
NA	Numerical aperture
NF	Noise figure
NRZ	No return to zero
OFC	Optical Fiber Communication, Conference
PMD	Polarization mode dispersion
QCE	Quantum conversion efficiency
RIN	Relative intensity noise
RZ	Return to zero
SDH	Synchronous digital hierarchy
SDM	Spatial division multiplexing
SHB	Spectral hole burning
SM	Single-mode
SNR	Signal to noise ratio
TDM	Time division multiplexing
WDM	Wavelength division multiplexing

1 INTRODUCTION

The need for fast Internet access for web browsing and other broadband applications, such as video on demand and video conferencing, initiated the investigation into high capacity optical networks for metro and access areas[1,2]. The excellent transmission properties of optical fibers together with dense wavelength division multiplexing (DWDM) and erbium doped fiber amplifier (EDFA) technology enables transmission speeds exceeding 10 Tbit/s[3] and transmission over distances of thousands of kilometres without repeaters[4]. The differences between requirements of the trunk and access networks demand improvment of the components, transmission systems and network structures[5,6].

The large range of different traffic types, the need for quick upgrade of connections, and the capability for future upscaling require fine granularity and agility from the access network[6,7]. As an example the Internet generates packet data transmission bursts. It is inefficient to carry this kind of data using time domain multiplexing (TDM) technologies like synchronous digital hierarchy (SDH) which was developed originally for carrying voice services[8]. Due to a smaller customer base the use of optics in metro area and access networks requires low cost of components, node element assembly and network management. One important difference between the trunk network and the metro area networks (MAN) is also the link distance, the typical node spacing in the MAN is 5-15 km[9]. This means that the optical nodes are the main source of optical losses in the network.

Kao and Hockham[10] published in 1966 their theoretical analysis illustrating the ability to transmit light over long distances using glass optical fiber. Kapron et al.[11] proved it experimentally at 1970 using silica glass fiber. When the semiconductor laser was introduced in early 1960[12], all the building blocks for the point-to-point optical fiber link were at hand. The era of fiber optics started, when TDM technology enabled the multiplexing of a large number of telephone conversations into a single transmission line between the exchanges thus creating the market for high-speed long haul transmission.

The optical fiber amplifier was introduced already in 1964 when Koester and Snitzer built the first fiber amplifier[13]. The first silica based erbium doped fiber (EDF) was introduced in 1985 by S. Poole et al. at Southampton University[14]. The breakthrough in the fabrication of the EDF was the use of the solution doping developed by J. E. Townsend et al.[15]. The EDFA based on this EDF was presented by R. J. Mears et al. in 1987[16]. The direct nanoparticle deposition (DND) process, introduced in 2001 by Liekki Oy[17], improved the doping process. The outcome of this was shorter and more economical EDFs for optical amplifiers[18] with enhanced performance[III].

The technology developed for the fabrication of telecom silica fibers gives an economically sound technology base for EDFA. The mechanical and environmental properties of the silica based EDF match well with proven silica based optical fibers[19]. A silica based host provides high efficiency to EDF because the position of the multiphonon edge in silica prevents optical output from possible transitions other than the main emission at 1550 nm[20]. At the conventional wavelength band (C-band, approx. 1530 nm – 1560 nm) the intrinsic gain flatness of the aluminium rich EDF is over 20 nm[20,21] and can be extended to over 30 nm in bandwidth using proper filtering techniques[19,21]. The use of the long wavelength band (L-band, approx. 1560 nm – 1605 nm) doubles the gain bandwidth by using the same mature technology.

The rapid growth in Internet data transmission creates a need for high-speed low cost optical transmitters for optical access and the metro area networks. The directly

modulated distributed feedback (DFB) laser is an obvious candidate to this. Unfortunately the chirp of the DFB laser limits the transmission length[22,23]. The development of external modulators[24] and the integration of electro absorption modulators with laser diodes solve this problem for long haul trunk networks[25], however, due to the complicated structures the economics bars their use in metro and access networks. Accurate chirp measurement provides a method to analyse this problem and thus gives more detailed information both for the laser dynamics and for the system requirements[26,27]. Spectral filtering provides also a method to improve the dispersion tolerance, when directly modulated DFB lasers are used[28,29,30,IX].

Wavelength division multiplexing (WDM) provides a new aspect to the metro networks. The use of DWDM enables the use of the optical layer as a functional layer. The use of the optical layer provides a new way to improve the configurability and also adds the transparency of the network to different signal bit rates and data protocols such as the Internet protocol (IP), Asynchronous transfer mode (ATM) and Gigabit Ethernet[1,2,6,7]. The use of optical bypassing decreases the need for processing capacity and the port count of the routers since the routing can be done partially at the optical level[1,6].

The structure of the modern MAN is shown in Fig. 1. The network is divided into two parts; the distribution network and the feeder network[6,7]. WDM can be used to integrate the feeder and the distribution parts of the network in a manner not available earlier. The different types of services can be assigned e.g. to separate wavelengths and the aggregation of these diverse services can be done at the customer premises using passive optical components[7]. At the access node these wavelengths can then be processed or some of them can be optically routed to another node[6,7], which reduces the equipment costs.

The feeder network cable is often multifiber cable[2,6,7,31] which provides a possibility to use spatial division multiplexing (SDM) together with WDM[2,31,32,X].

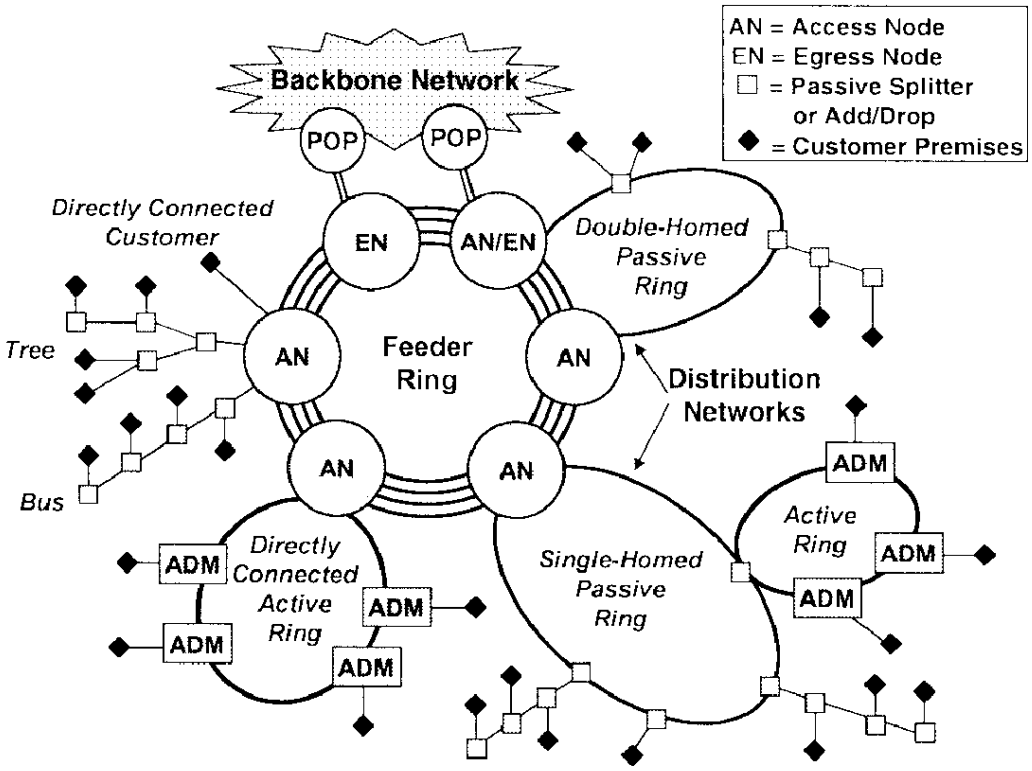

Fig. 1. An example of a regional metropolitan network consisting of distribution networks and a feeder network[6]. © 1999 IEEE.

1.1 The aims of this thesis

The target of this thesis is the study and the development of the key technologies that enable the use of optical transmission in metro area and access networks. Specifically the target areas are optical amplification, low cost high-speed transmitters and metro ring networks.

The aim of the studies into optical amplification is to create a better understanding of the effects of non-idealities resulting from different processing steps, to find out methods to produce better and cost effective EDF and to examine how to lower the costs of manufacturing metro EDFAs containing the required control and management functions.

The main target for low cost high-speed transmitters is to find out better and cheaper ways to characterize the chirp of directly modulated lasers and study how this know-how can be used to improve the usability of the directly modulated laser in optical networks.

The study of metro ring networks is focused on the combinations of SDM and WDM together to realize a cost effective solution for the ring network.

2 ERBIUM DOPED FIBER

The solution doping method, the most commonly used process for making the EDF, is studied. By separating the soot growth and the sintering phase the uniformity of the porous layer is improved resulting in homogeneous doping in the fiber core[II]. The EDF structure is simulated in order to optimise the index profile of the EDF. The effects of the processing steps that result in non-ideal refractive index profiles are also taken into account in the simulations[I].

The recently developed DND technology is a nanoparticle glass forming process where the doping can be done simultaneously with glass formation[17]. The DND technology improves the uniformity of the doping resulting higher doping levels, shorter EDF lengths and lower polarization mode dispersion (PMD). This technology lowers the costs and simplifies the construction of the EDFAs while improving simultaneously the optical characteristics[18]. The shorter fiber length decreases significantly the sensitivity to optical non-linear processes, an important issue when building the L-band EDFA[III].

The coupling of the pump laser into a SM fiber is at present the most critical and expensive phase when constructing EDFA's. This costly coupling can be avoided by combining an additional large cross-section multimode waveguide for the pump light into the cladding of the EDF. This can be beneficial in L-band amplifier because it provides more uniform inversion in the EDF and thus improves the quantum conversion efficiency (QCE)[IV].

2.1 The EDF fabrication

Koester and Snitzer[13] built the first fiber amplifier with a side pumped neodymium fiber in 1963-1964, only a few years after the development of lasers. The fiber was made by cladding a Nd doped glass core with a lower index glass. This was before Kao and Hockham presented their studies illustrating the opportunity to use optical fibers for telecommunications in 1966[10]. Kapron et al. showed the possibility to fabricate silica based glass fibers having low optical loss in 1970[11], which proved the possibility to use optical fibers for telecommunication. J. Stone and C.A. Burrus continued the development of the fiber laser by introducing the solution doping method[33] and showing the possibility to use a semiconductor laser for end pumping the fiber laser in 1974[34].

S. Poole et al. in Southampton university demonstrated the fabrication method for quartz based doped fibers in 1985[14]. This manufacturing process was developed from modified chemical vapour deposition (MCVD) originally developed at Bell Labs by MacChesney in 1974[35]. In the MCVD process the reactive gases are fed into a silica tube. This tube is in a glass lathe where it is heated at one position using hydrogen / oxygen burner. In the hot region the gases, typically $SiCl_4$, $GeCl_4$, PCl_4 and O_2, react and form small sub-micron particles, soot, of silica glass doped with GeO_2 and P_2O_5. These particles flow due to thermophoresis to the wall of the quartz tube[35]. When the heater is slowly moved in the same direction as the gases the soot is sintered at the hot zone thus forming a thin transparent film of glass. When several layers of glass films have been grown in the tube, it is collapsed into a glass rod. The grown glass layers form the guiding part of the fiber preform.

Unfortunately this method was not compatible to handle halides such as rare earth halides, which have very low vapour pressures at room temperature. To circumvent this problem S. Poole et al.[14] used a separate part of the silica tube as a container for the rare earth source, see Fig. 2. The container part of the tube was heated separately to control the

$ErCl_3$ content in the tube. The temperature of the silica tube was high enough for $ErCl_3$ to remain in the gas phase and to react at the hot zone to form Er_2O_3.

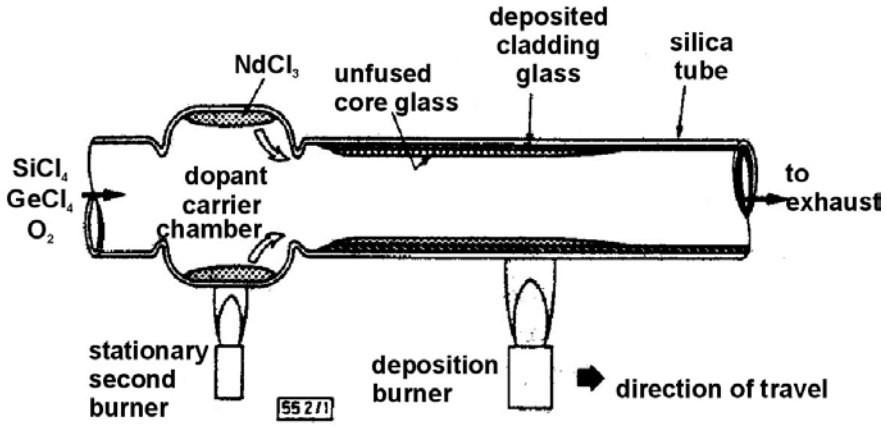

Fig. 2. Fabrication set up for rare earth doping using MCVD, Poole et al.[14], © 1985 IEEE.

In 1987 the solution doping technique was adapted to this technology again at Southampton University by J. E. Townsend et al.[15], see Fig. 3. R. J. Mears et al. from the same group demonstrated an EDFA in 1987[16]. In this modification a porous layer of doped silica glass is processed on the inner side of a quartz tube using the MCVD technology. Using lower temperature at the hot zone, the soot layer formed a porous frit, which is hard enough to be soaked in water containing $ErCl_3$ and other dopants, like $AlCl_3$, $YbCl_3$[20]. After soaking the preform into water it is dried and attached back to the glass lathe. When the chlorides with their crystalline water, like $ErCl_3 \cdot 6(H_2O)$, are heated they form first hydroxides, like $Er(OH)_3$, and hydrochloric acids, HCl. When the temperature is further increased the oxides are formed and the extra water is released. Finally the temperature is increased so that the dopant oxide is diffused into silica glass and the glass is sintered.

The method of counter-propagating the burner and the halide precursors was used in the EDF processing in publication II. This enables the use of high processing temperature at the reaction zone because the partial sintering of the soot layer is done at a separate process phase. The uniformity of the frit was controlled in the pre-sintering densification process using the colour of the light scattered from the partially sintered frit. The variation of the aluminium concentration was below 20 %. The same idea of translating the burner in direction opposite to the halides has also been developed separately in processing high phosphorous-doped glass frit for solution doping[36].

The solution doping process relies on uniform porous glass soot and there is no direct feedback during the partial sintering phase. This makes it difficult to control the rare earth doping level and homogeneity of the dopant profile. This problem started the development of the DND process[17,18]. In the DND process the precursor solution is fed in liquid phase directly to the reaction zone, Fig. 4a. The clustering tendency is low in this process because the glass is doped in-situ with the glass particle formation. Furthermore, the DND process makes it possible to mix the index difference forming materials with other dopant materials already during the deposition of the glass particles. This results in excellent homogeneity of the glass composition in the porous glass soot preform that is sintered in the next phase into a solid glass tube. Finally the tube is collapsed into a solid core rod and sleeved with a pure silica glass tubes, which forms the cladding. Fig. 4b shows a radial dopant concentration profile of a preform.

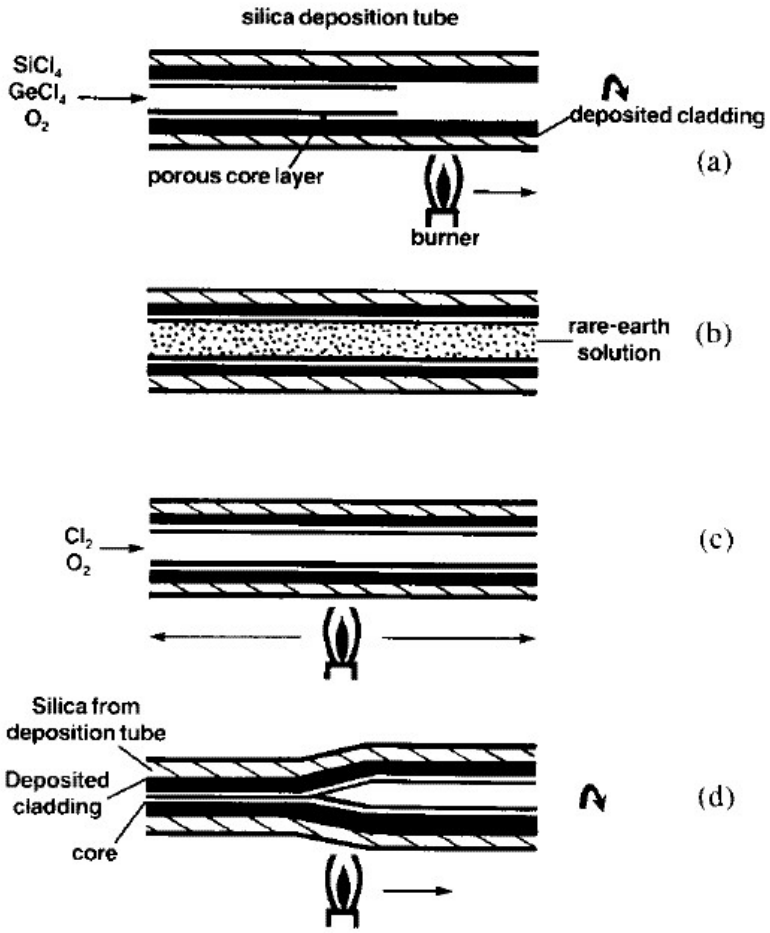

Fig. 3. Fabrication set up for rare earth doping using MCVD and solution doping by J. E. Townsend et al.[15], picture from[20], © 1991 IEEE.

a) *b)*

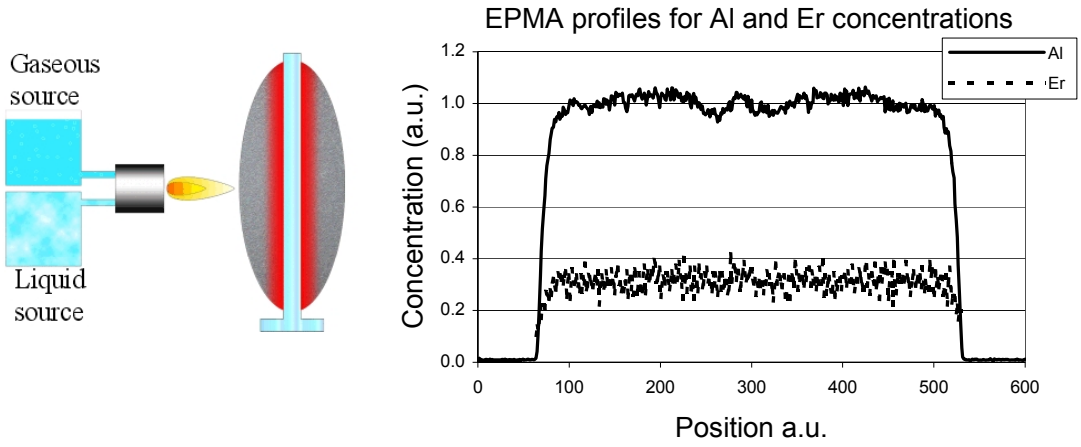

Fig. 4. a) DND process equipment[18], b) Radial erbium and aluminium profiles in the core of the DND preform. The Er-profile is multiplied by 10 compared to the Al-profile[18].

2.2 Modelling

In a glass host the surrounding crystal structure causes a Stark splitting of the Er^{3+} orbitals, Fig. 5 and Fig. 6. The homogeneous broadening of the transitions over the Stark split manifolds of the laser transitions of the rare-earth ions generally exceeds the inhomogeneous broadening in glass due to the broadening effect of phonon coupling[38]. This assumption simplifies the simulations and agrees excellently with the experimental results[39]. The probability of absorption η_a and stimulated emission η_e for a single atom between the laser levels $^4I_{15/2}$ and $^4I_{13/2}$ can be described using absorption and emission cross-sections, σ_a and σ_e.

$$\eta_a = \sigma_a(\upsilon)N_1\Phi(\upsilon)\,,\ \eta_e = \sigma_e(\upsilon)N_2\Phi(\upsilon)\,. \tag{1}$$

Here υ is the frequency of the light, $\Phi(\upsilon)$ is the photon flux at frequency υ at the atoms site, N_1 and N_2 are the fractional populations of the lower ground state, $^4I_{15/2}$ and the upper excited state, $^4I_{13/2}$, respectively. The Er can be considered as a two level atom and no excited state absorption is needed to account for the most common pump wavelengths (980nm and 1480 nm)[38,40]. The rapid relaxation from $^4I_{11/2}$ to $^4I_{13/2}$ simplifies the simulation when 980 nm pumping is used; only the absorption due to the transitions from $^4I_{15/2}$ to $^4I_{11/2}$ has to be taken into account. This results $N_1+N_2=1$. The time derivative of the population at upper level N_2 is then

$$\frac{dN_2(t,r,\theta,z)}{dt} = -\frac{N_2(t,r,\theta,z)}{\tau} +$$

$$\int_{\upsilon=\upsilon_{\min}}^{\upsilon_{\max}} \left\{\left[\sigma_a(\upsilon)N_1(t,r,\theta,z) - \sigma_e(\upsilon)N_2(t,r,\theta,z)\right]\Phi^{\pm}(\upsilon,r,\theta,z)\right\}d\upsilon\,. \tag{2}$$

Here r is the radius from the fiber centre, θ is the azimuth angle, z is the position from fiber end, τ is the lifetime of the excited state, and $\Phi^{\pm}(\upsilon)$ is the photon flux at frequency υ. The integration goes over the frequency region where there is absorption and / or emission and includes beams propagating in both directions.

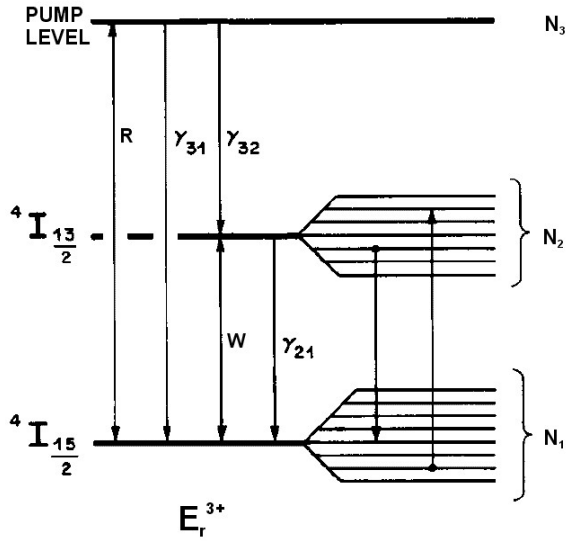

Fig. 5. Relevant energy levels of an Er^{3+} ion including the Stark splitting[38], © 1989 IEEE.

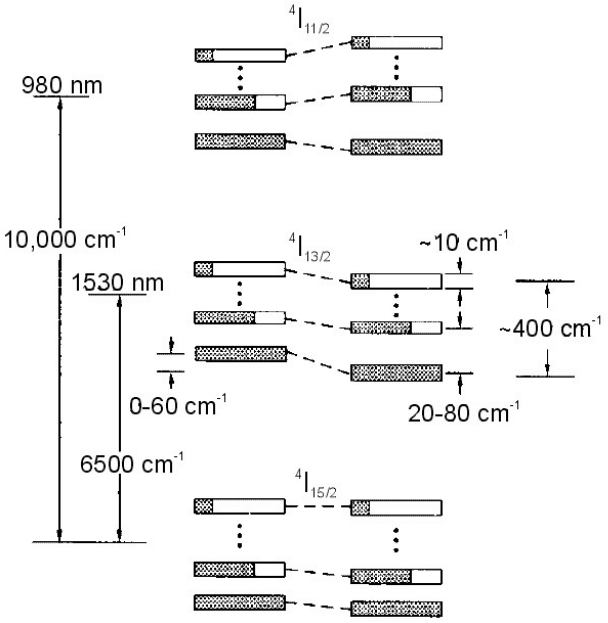

Fig. 6. Shading represents the room-temperature Bolzmann-distributed populations of each manifold[41]*, © 1991 IEEE.*

In order to cover the effects of the waveguide structure and the consequent modal field distributions the local inversion in all three dimensions is taken into account[42]. The photon flux can be described by using the radially symmetric normalized optical power distribution of the mode $\psi(\upsilon,r)$ and the number of photons at that frequency in the mode $\zeta(\upsilon,z)$. The $\psi(\upsilon,r)$ is normalized so that $\int_0^\infty \psi(\upsilon,r)2\pi r dr = 1$

$$\Phi(\upsilon,r,\theta,z) = \zeta(\upsilon,z)\cdot\psi(\upsilon,\theta,r)\,. \tag{3}$$

Using these equations and assuming the Gaussian distribution for the pump and signal intensity it is possible to optimise the confinement of the pump and signal modes[43]. When the more accurate power distribution is needed, the electrical field distribution ψ_e of the EDF can be calculated directly from the refractive index distribution using the scalar wave equation,

$$\left[\frac{d^2}{dr^2}+\frac{1}{r}\frac{d}{dr}+\left\{k^2n^2(\upsilon,r)-\beta^2(\upsilon,\nu)-\frac{\nu^2}{r^2}\right\}\right]\psi_e(\upsilon,r)=0\,. \tag{4}$$

In this equation $k = 2\pi n\upsilon/c$ is the wave number, n is the refractive index, ν is the angular mode number, (e.g. for LP_{01} $\nu = 0$ and for LP_{11} $\nu = 1$), and β is the propagation constant of the mode. The optical power or the photon distribution is proportional to the square of the electrical field distribution.

The index profile of the fabricated EDF is very seldom as designed. Often in the centre there may be an index dip and the diffusion of the dopants takes place at the processing stage. Using the scalar wave equation for defining the field distribution, it is possible to study the influence of these index profile nonidealities formed in the processing stages. In publication I the effects of the index dip, the diffusion of the dopant materials, and the confinement of the waveguide mode on EDF performance are studied.

When the concept of local capture fraction[39] for spontaneous emission is taken into account, the model can also account the noise properties of the EDFA[39]. The local capture

fraction $\Omega^{\pm}$ defines the probability of a spontaneously emitted photon coupling to the waveguide mode

$$\Omega^{\pm} = 1/\left(8\pi^2\right)\cdot\left(\lambda/n\right)^2\cdot\psi(\upsilon,r) \tag{5}$$

When the local populations are considered as time variant this model can be used for accurate analysis of the dynamic effects in the EDFA[44].

The assumption of totally homogeneously broadened Stark splitting is not exactly valid, the small amount of inhomogeneous broadening causes some spectral hole burning (SHB) in the gain spectrum. The SHB has to be taken into account when the EDFA is heavily saturated or the gain spectrum is important. For example, the SHB must be taken account in systems where the gain of the EDFA is clamped using an all optical feedback loop[45] or there are a large number of EDFAs in fiber link[46].

In the optimised fibers the variations of the signal and pump power mode distributions across the Er^{3+} doped area can be considered small and thus the radial dependence of the Er^{3+} inversion level can be neglected. This can be used to simplify the equations, for this we define absorption α_a and emission α_e constants of the EDF:

$$\alpha_a(\upsilon) = \rho^*\Gamma(\upsilon)\sigma_a(\upsilon)\,,\ \alpha_e(\upsilon) = \rho^*\Gamma(\upsilon)\sigma_e(\upsilon)\,, \tag{6}$$

$$\rho^* = \frac{\int_0^{r_d}\rho(r)2\pi r dr}{\pi r_d^2}\,. \tag{7}$$

Here the ρ^* is the average erbium concentration in the fiber and r_d is the radius of the doped area. The confinement factor Γ is the overlap integral between the optical intensity profile and the erbium concentration distribution $\rho(r)$:

$$\Gamma = \frac{\int_0^{\infty}\psi(r)\rho(r)2\pi r dr}{\rho^*}\,. \tag{8}$$

When the amplified spontaneous emission (ASE) is neglected and the fractional populations N_1 and N_2 are considered as uniform across the core region, e.g. not depending on radius r or the azimuthal angle θ, equation (2) can be rewritten using the optical powers of the different signal and pump beams, P_k[47]. The powers are expressed here in number of photons per unit of time.

$$\frac{dN_2(z,t)\rho^* A}{dt} = -\frac{N_2(z,t)\rho^* A}{\tau} - \sum_{k=1}^{N} u_k\frac{\partial P_k(z,t)}{\partial z}\,. \tag{9}$$

In this equation A is the core area and u_k gives the direction of the corresponding beam. u_k is 1 when the beam enters at z = 0 and -1 otherwise. Now we can integrate (9) from beginning to end of EDF (0 to l).

$$\left(\frac{d}{dt}+\frac{1}{\tau}\right)l\overline{N_2}(t)\rho A = P^{out}(t) - P^{in}(t)\,. \tag{10}$$

Here $P^{out}(t)=\sum_{k=1}^{N}P_k^{out}(t)$, $P^{in}(t)=\sum_{k=1}^{N}P_k^{in}(t)$ and the $\overline{N_2}(t)$ is defined as the averaged fractional population of the upper level in the EDF,

$$\overline{N_2}(t)=\frac{\int_0^l N_2(z,t)dz}{l}. \tag{11}$$

In the steady state situation ($\overline{dN_2}/dt=0$) the averaged upper level population can be expressed:

$$\overline{N_2}=\frac{\tau(P^{out}-P^{in})}{\rho^* A}\cdot\frac{1}{l}. \tag{12}$$

On the other hand the change of the optical power in k-th beam in the EDF can be stated also using absorption and emission cross-sections[47]:

$$\frac{\partial P_k(z,t)}{\partial z}=u_k\left[\left(\alpha_e(\upsilon_k)+\alpha_a(\upsilon_k)\right)N_2(z,t)-\alpha_a(\upsilon_k)\right]P_k(z,t). \tag{13}$$

We can now rewrite the (2) into form,

$$\frac{dN_2(z,t)}{dt}=-\frac{N_2(z,t)}{\tau}-N_2(z,t)\sum_{k=1}^{N}\frac{\alpha_e(\upsilon_k)}{\rho^*}\frac{P_k(z,t)}{A}+N_1(z,t)\sum_{k=1}^{N}\frac{\alpha_a(\upsilon_k)}{\rho^*}\frac{P_k(z,t)}{A}. \tag{14}$$

In the steady state situation the fractional upper level population N_2 is:

$$N_2=\frac{\sum_{k=1}^{N}\alpha_a(\upsilon_k)P_k(z,t)}{\frac{\rho A}{\tau}+\sum_{k=1}^{N}\left(\alpha_a(\upsilon_k)+\alpha_e(\upsilon_k)\right)P_k(z,t)}. \tag{15}$$

By integrating the equation (13) we can couple the input and output power of the beam k with the averaged upper level population,

$$P_k^{out}=P_k^{in}\exp\left(-\alpha_a(\upsilon_k)l\right)\cdot\exp\left(\overline{N_2(t)}\left(\alpha_e(\upsilon_k)+\alpha_a(\upsilon_k)\right)l\right). \tag{16}$$

Now combining (12), (16) we have a single transcendental equation describing the absorption and gain in EDF:

$$P^{out}=\sum_{k=1}^{N}P_k^{in}\exp\left(-\alpha_a(\upsilon_k)l\right)\cdot\exp\left(-\frac{P^{in}}{P_k^{IS}(\upsilon_k)}\right)\cdot\exp\left(\frac{P^{out}}{P_k^{IS}(\upsilon_k)}\right). \tag{17}$$

The $P_k^{IS}(\upsilon_k)$ used here is the intrinsic saturation power, given in the following equation[47].

$$P_k^{IS}(\upsilon_k)=\frac{A\rho}{\left[\alpha_e(\upsilon_k)+\alpha_a(\upsilon_k)\right]\tau}. \tag{18}$$

When the input powers, absorption and emission cross-sections are known the output power to different light beams can be calculated using (9).

Equations (10) and (13) also form a single ordinary differential equation describing the time dependant behaviour of the EDFA[48]. This equation can be further simplified and an analytical model has been formed using Laplace transformations[49]. However, this analytical model can be used only for small or medium input power variations.

In network modelling there is a need for a simple and fast EDFA model. The dynamic gain tilt technique or black box model, similar to the average inversion level method shown above, uses two EDFA gain measurements[50]. The measurements are performed using different input saturating signal levels. The saturating signal has the same wavelength at both measurements and the gain spectrum is measured using a small probing signal. When the gain spectrum is known at two different upper fractional populations N_2, and the optical power that generate these two gain spectra are known, the gain spectra in power levels between these two situations can be calculated. This dynamic gain tilt model also provides an efficient tool to extract the gain coefficient of EDF from the two EDFA gain measurements[51,52]. This method is suitable especially in the L-band region, where the gain is low compared to the gain at C-band.

When the erbium concentration is increased the erbium ions start to couple with each other. This results concentration quenching, which comes from cooperative upconversions. The upconversion process is a result of nonradiative energy transfer due to electric multipolar interactions, Fig. 7. In the starting point both of the ions are in the excited state $^4I_{13/2}$. After the interaction the donating ion is transferred to the ground state, $^4I_{15/2}$, and the acceptor ion is transferred to the $^4I_{9/2}$, from which it relaxes to the metastable state, $^4I_{13/2}$. The energy of the excited donor atom is lost to phonons in this process. The upconversion processes are divided into two categories, the homogeneous and the inhomogeneous. The homogeneous upconversion is a result of overall interionic distances in the glass network. In inhomogeneous upconversion the erbium ions have formed clusters comprised of two or more erbium ions.

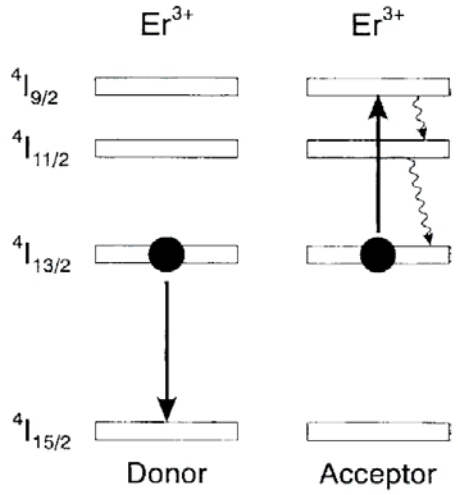

Fig. 7. The energy diagram of erbium ions in the upconversion process[53], © 1997 IEEE.

The absorption and emission cross-sections and spontaneous emission rate can be considered to be the same for the erbium ions, whether they are clustered or not[53]. The time constant of the upconversion process in an ion cluster is very short compared to the isolated erbium ion. Only one of the ions in a cluster can be excited, all the extra excitations result immediate upconversion and lost of optical power. If the size of the cluster is m ions (m is larger than 1) then the fractional upper level population of the clustered ions N_{c2} can be written[53]

$$N_{c2} = \frac{\sum_{k=1}^{N} \alpha_a(\upsilon_k) P_k(z,t)}{\frac{\rho A}{\tau} + \sum_{k=1}^{N} \left(m\alpha_a(\upsilon_k) + \alpha_e(\upsilon_k)\right) P_k(z,t)}. \quad (19)$$

Generally it is considered that the ions form mainly clusters of two ions, ion pairs, and this assumption is used when calculating the amount of clusters in EDF[53].

Homogeneous upconversion can be taken into account by including a term $-k_2[N_2(r,\theta,z)]^2$ for two particle and $-k_3[N_2(r,\theta,z)]^3$ for three particle homogeneous upconversion on the right hand side of equation (2)[53]. However, it is shown, that this approximation is not valid for high inversion situations[54]. In order to propely model homogeneous upconversion the proximity of the erbium ions in silica glass matrix also has to be taken into account along with the migration of the excited state[55]. Due to the high increase of homogeneous upconversion at high inversions it is almost impossible to distinguish these two processes from the results of the gain measurements.

2.3 The characterisation of EDF

In principle the gain and absorption spectrums are straightforward to measure. With low optical powers one can measure the absorption spectrum and with high pump power the gain spectrum. Unfortunately the low power creates problems when measuring the weak signals accurately. The pump power levels required to achieve total inversion are high, several hundreds of milliwats, and are not always available.

When designing the measurement set-up and procedures there are some rules of thumb. When the gain of the EDFA is less than 20 dB or the total input signal power is greater than –20 dBm, gain saturation due to ASE is negligible[47]. The transit time of the EDF is rather fast (0.1-10ms), and can thus be neglected in most steady state measurements[47,48].

For the measurement of the gain spectrum a short length of EDF is heavily pumped, so that the whole length of the EDF is almost totally inverted. The fiber length is short so that the total gain is well below 20 dB and thus the signal and the ASE power levels remain low enough not to saturate the EDF[56]. With the help of simulation it is possible to improve the measurement accuracy when using lower pump power levels[50,51,52]. Succesfull simulation, however, requires information on the refractive index profile and the overlap integral between the mode field and the doped region[41].

In the EDF analysis the Er^{3+} concentration distribution is either assumed to be known or it is measured using X-ray microprobe analysis[20,56]. The spatial resolution of this measurement is not good enough for measuring directly the EDF; it is done either from the preform or from a thick EDF piece drawn for this purpose. The mode field diameters of EDF can be measured using standard methods.

Another method of measuring the ratio between the emission and absorption cross-sections is to measure the gain as a function of pump power. By using the unknown ratio of the absorption and emission cross sections as a fitting parameter the theoretical gain dependence is then fitted to the measurement results[56]. The Fuchtbauer-Ladenberg analysis can be also used to calculate the ratio between the two cross-sections[56]. Unfortunately the results differ from more direct loss-gain measurements. A possible reason for this could be that all the transition probabilities between different Stark states are not equal[56]. The reciprocity between the absorption and emission cross-section developed by McCumber[57] shows good fit between the measured absorption and emission cross-sections[40].

$$\sigma_a(\upsilon) = \sigma_e(\upsilon)\exp\left[\frac{h(\upsilon-\varepsilon)}{k_B T}\right]. \quad (20)$$

Here ε is the frequency, where the absorption cross-section equals the emission cross-section, and T is the ambient temperature. Because the accuracy of absorption measurement is better than the accuracy of the gain measurement, especially at L-band, this equation can be used to improve the emission cross-section measurement.

One method of measuring the intrinsic saturation power P^{IS} is the use of a step like pulsed high power signal[58]. In this method the output of the EDF is studied in the time domain. At the beginning of the signal pulse the Er^{3+} ions are in the ground state, and the absorption of the EDF is unsaturated. As the signal power stays on the upper laser level, population starts to increase and the absorption is partially bleached. When the pulse ends, the fluorescence from the excited ions can be measured. By measuring the fluorescence time constant, the time constant of the change in absorption at the start of the pulse, the output power levels at the beginning and the time when the absorption is saturated, the intrinsic saturation power P^{IS} can be calculated[58].

The lifetime of the excited state can be measured straightforwardly using a pulsed pump source and fast detector[59]. If there is possibility of homogeneous co-operative upconversion in the EDF it exists only at high inversion levels. In order to see these fast-decaying processes high power pump pulses must be used[59].

The lifetime measurement can be done in the frequency regime; the pump laser is modulated with sinusoidal signal and the spontaneous signal is measured using synchronous detection. Then the modulation frequency is swept and the lifetime response is collected. This synchronous detection improves the sensitivity of the measurement and spontaneously emitted light from fiber side can be measured[60].

2.4 EDF optimisation

Several aspects have to be considered when optimising the EDF: efficient coupling to standard fibers, good QCE, low noise figure (NF), high gain and broad gain bandwidth. Efficient coupling can be realised using the same waveguide parameters for the EDF as are used for the standard fiber. This, however, is quite contradictory to optimising other factors, which favour high numerical aperture (NA) and small core diameter[62]. This can be resolved to some extent using tapered structures based on either core material diffusion during fusion splicing[63] or physically tapering the fiber[64,65]. Low NF, high bandwidth and high gain can be achieved almost simultaneously with high NA EDF having rather low V-values (1.2 – 1.6)[I,39,66,67]. The composition of the host glass plays also an important role; the highest gain is achieved with only Ge doping[66] and the broadest natural bandwidth, up to 20 nm, with highly Al doped host glass[20,21,56], Fig. 8.

The increase of the NA from 0.15 to 0.25 improves the QCE by 9% when the pump power is 100 mW. The Er^{3+} confinement improves QCE only by 2% when the NA is 0.25 and the pump power is 100 mW[68].

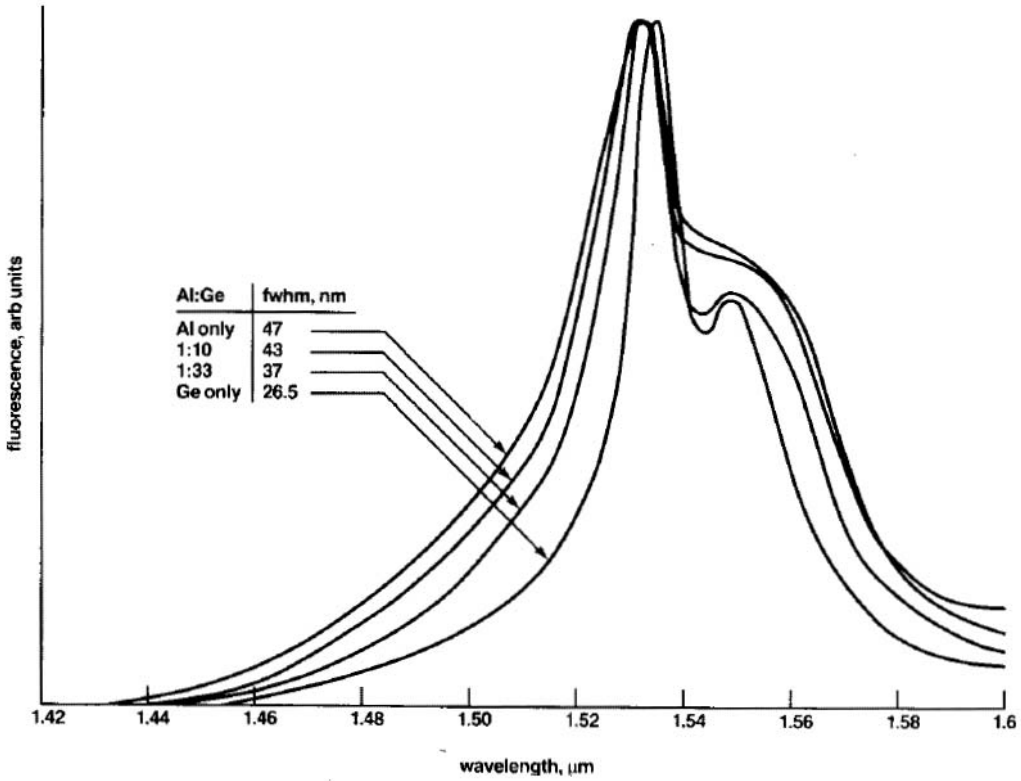

Fig. 8. Fluorescence curves for different host glasses20, © 1991 IEEE.

The processing steps that result in non-ideal refractive index profiles need to be taken into account when comparing different processing schemes and EDF compositions[39,66,I]. Due to the volatility of doping materials, e.g. germanium oxide, an index dip may form in the centre of the core during the collapsing process. In addition diffusion of the doping materials takes place during the collapsing phase. E.g., a dip having a width of 75% of the core diameter and a depth of 100 % from the index difference degraded the gain of the EDF about 37%[I]. On the other hand the diffusion of the dopants at the interface between the core and the cladding had only a minor effect on the gain. The shape of the index profile also slightly changes the optimum cut-off wavelength of the EDF[I].

There is also a long list of processing parameters that change the EDF properties, e.g., the amount of thermal processing (clustering, crystal growth), drying gases and temperatures (e.g. Cl induced scattering) and drawing parameters (drawing induced losses)[20,36,66,II].

2.5 L-band Er doped fiber

The L-band amplifiers use the same mature technology that is used in C-band EDFAs. Usually the C-band and L-band are defined respectively as 1528 nm – 1562 nm and 1570 nm - 1605 nm. The L-band corresponds to the tail of the $^4I_{13/2}$ – $^4I_{15/2}$ energy level transition[69]. Due to the use of the tail, the emission and absorption coefficients are 3-4 times smaller than in the C-band. In order to minimise the high intrinsic gain at C-band, the L-band EDFA operates at a low average inversion[69]. As a result of these operation conditions, the length of the EDF is 7-10 times longer than in C-band EDFA.

Fiber non-linearity is often considered as the limiting factor in DWDM systems. The small effective area of the EDF and the long lengths used in L-band EDFA have also brought this limitation to L-band EDFA, mainly due to four-wave mixing (FWM)[70,71,72]. The FWM efficiency is less sensitive to channel spacing in EDF due to shorter interaction length than in the transmission single-mode (SM) fiber[70]. The FWM depends quadratically on fiber length and thus L-band EDFAs benefit from having high erbium

concentration[70,III]. PMD is another limiting factor in L-band amplifiers and managing this is also easier when the EDF is kept short.

The required EDF length can be reduced by increasing the erbium ion concentration or by increasing the relative doped area of the core. However, concentration quenching due to upconversion processes limits the maximum concentration[53]. All the non-uniformity in concentration, like clustering, result in higher upconversion and thus decrease in efficiency. The non-uniformity in concentration is a result of the glass synthesis process in addition to the glass chemical composition. The DND process makes it possible to reduce the EDF length in L-band EDFAs from conventional 50-100m to about 12m[III]. This decreases notably the FWM and PMD, while keeping the QCE over 40 % when measured for the L-band[III].

Like C-band EDF the L-band EDF has inhomogeneous gain saturation affecting the spectral characteristics. The SHB is much higher in Ge-doped EDF[73] than in highly Al-doped EDF[III], where the SHB is barely measurable.

2.6 Double Cladding (DC) EDF

High power, low cost and spatially multimode broad stripe lasers can be used for pumping the DC EDF. Because the pump waveguide is remarkably larger than the core of the SM fiber, the coupling from the pump laser chip to pump waveguide can be realised using simple, low cost and robust techniques[74,75,76]. The high pump power makes it possible to realise high power amplifiers[74,75,76,77,78,79] and lasers[80,81,82].

The first DC doped fiber structure was demonstrated by H. Po et al. already in 1989[82]. In this structure the second cladding was formed from a polymer. The use of the polymers on the second cladding may create a reliability problem. The coupling to a more standard silica fiber is also complicated. These problems can be avoided by making an all-glass structure using fluorosilicate glass[36]. Unfortunately the achievable refractive index difference is reduced with these all-glass structures. Another possible solution is the use of holey fiber structures in the pump waveguide cladding, where the glass air interface provides high refractive index to the all-glass DC fiber structure[37].

The schematic structure of the DC EDF is shown in Fig. 9. In the DC EDF the doped single mode waveguide is surrounded by a multimode waveguide. The surrounding multimode waveguide guides the pump light thus operating as the pump waveguide.

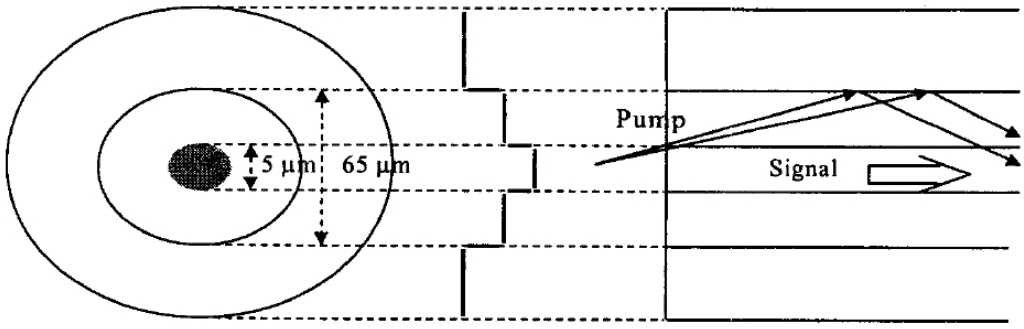

Fig. 9. The schematic picture of the DC EDF78, © 1999 OSA.

The DC EDF can be modelled using the same concepts and equations as single cladding EDF, except for the overlap of the pump light, which propagates in a highly multimode waveguide. If the shape of the pump waveguide cross-section provides uniform distribution to all modes, the local pump photon density is the pump power divided by the

pump waveguide area[IV,83]. This doesn't apply for a circular pump waveguide. There the skew modes don't have any power in the centre region of the pump waveguide, where the doped waveguide is.

In publication IV we studied the optimisation of the pump waveguide cross-sectional area of DC EDF for L-band EDFAs. The relation between the pump waveguide area and the signal waveguide area impacts the probability of the absorption of the pump light. This can be exploited in L-band amplifiers[IV]. The decreased absorption results in a more uniform inversion in the EDF and improves the QCE of the L-band amplifier when 980 nm pumping is used[IV]. By changing the area of the pump waveguide, the pump absorption can be adjusted and the operation of the EDFA can be optimised, see Fig. 10.

Co-doping the fiber with Yb^{3+} increases the absorption of the low brightness, broad stripe pump laser light. The energy of some of the excited Yb^{3+} then migrates to Er^{3+} thus exciting it. The absorption of the pump light and the excitation of the Er^{3+} are accomplished by the Yb^{3+} ions. The Yb^{3+} ions have large absorption cross-sections and the very high doping level compensates the low pump absorption due to the high area ratio between the signal and pump waveguides[79].

In Yb^{3+} co-doped EDF a rather high P_2O_5 concentration is required to provide rapid multiphonon decay from the $^4I_{11/2}$ level of Er^{3+}. This minimises the back-transfer of the energy from Er^{3+} to Yb^{3+} ion[79,36]. The drawback using P_2O_5 is that the gain spectrum of Er^{3+} is not as broad as when using Al_2O_3 doping. The Yb^{3+} co-doping also reduces the pump wavelength tolerance due to the broad absorption band at 920 nm[79].

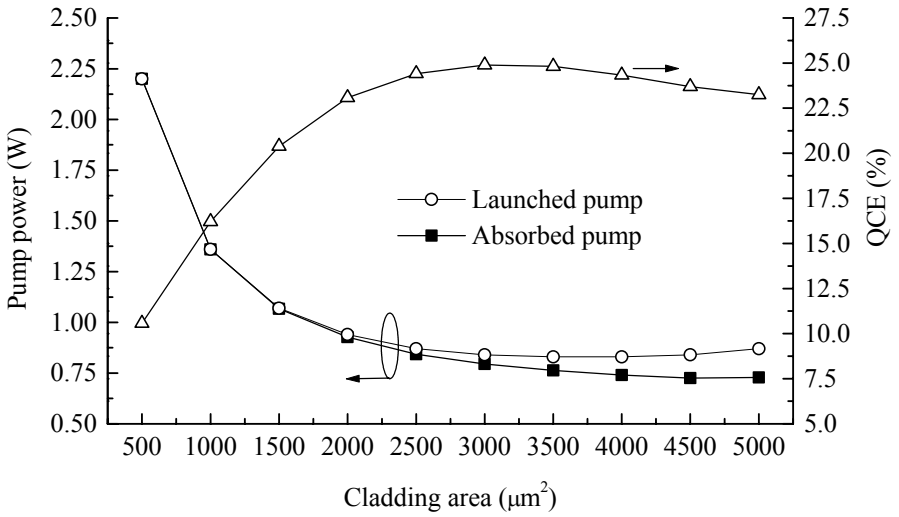

Fig. 10. Launched and absorbed pump power and QCE as a function of cladding area. Gain is fixed at 20 dB for a 0-dBm signal at 1590 nm[IV], © 2001 IEEE.

The efficient coupling of the pump light to the pump waveguide in DC EDF can be done using the existing WDM technology common to DWDM single wavelength add/drop components[74,84]. A more elegant solution is to fuse and taper a bundle of multimode fibers and one SM fiber to form a fused multimode coupler, where the outer fibers create coupling to pump waveguide, while the SM fiber in the centre couples the signal to the centre core waveguide[76]. A simpler means to couple the pump power to DC EDFA is the use of side pumping[75,85,86,87]. In this method a polished V-groove is created in the DC EDF and the pump light is coupled via total internal reflection from the facets of this V-groove.

The NF of the cladding pumped EDFA is usually worse than that of the more common transversally single-mode-pumping scheme. This can be improved by using a separate pre-amplifier[76,78]. Another method is to use a specially designed ring doping structure[83]. Only the ring area around the core center is doped, where the brightness of the signal mode is low. Now the pump brightness remains higher compared to the amplified signal in the doped region. This keeps the population inversion high and improves the NF. A broad and flat gain bandwidth of 30 nm at L-band has been also demonstrated using Yb^{3+} co-doped DC EDF[78].

3 ERBIUM DOPED FIBER AMPLIFIER

The characterization of the EDFA accounts for a large portion of the manufacturing cost. The gain and the ASE at the saturating signal wavelength decreases due to SHB. In order to measure the NF precisely the ASE should be measured at the signal wavelength. The large deviation of the optical powers between the signal and ASE makes direct measurement difficult[88]. The long lifetime of the excited state of the erbium ion makes it feasible to use temporal filtering for separating the signal and noise at the same wavelength[89,IV]. The measurement set-up using temporal filtering was realised using simple and low cost components yielding accurate and fast measurements[IV].

The use of DWDM technology in the MAN requires flexible adding and dropping of wavelength channels. As the EDFA operates normally in saturation regime, the gain depends on the input signal power. The input power of the EDFA is successfully used to regulate the pump laser and this feed-forward control scheme provides a simple, low cost controlling and managing system for EDFA in MAN applications[VI].

3.1 EDFA measurement

The most important characteristics of EDFA are the gain and the NF_{ASE} as a function of input power and wavelength[88,90]. The interference between the signal and the ASE produce the NF_{ASE}. The other noise component, which is generated from the interference between the ASE with itself, is most often negligible in practical systems. The reason for this is the use of DWDM filters before the receiver or the high signal level at the EDFA input. The NF_{ASE} can be calculated from the measured gain, G, and ASE power, P_{ASE}, of the amplifier, equation (21).

$$NF_{ASE} = \frac{P_{ASE}/B_0}{h\upsilon \cdot G} + \frac{1}{G} \tag{21}$$

The B_0 is the optical bandwidth in the frequency domain where the P_{ASE} is measured.

The P_{ASE} must be measured exactly at or very close to the signal wavelength. Unfortunately the high power amplified signal disturbs the measurement substantially[88]. The methods used to measure the ASE close to signal are curve fitting of the measured ASE spectrum and interpolation[91], polarisation-nulling of the signal[90], the pulsed source technique[92] and temporal filtering[89,V].

In the polarisation nulling technique it is assumed that the ASE noise is randomly polarised. The signal used has only one polarisation state, which is true for most transmitters. A polariser is used to filter out the amplified signal so that the ASE noise at the other orthogonal polarisation state can be measured at the same wavelength as the signal[90]. The result is valid only when there is no polarisation dependency in the EDF.

In the pulsed source method the input signal is pulsed using a separate chopper[92]. The output is then fed through a spectrum analyser and analysed in the time domain using a fast detector. From the time point, when the signal is cut off, the ASE starts to grow in an exponential manner. The ASE level at the time when signal was on can be derived by extrapolating the evolution of the ASE level to the time when the signal was cut off. Using this method the NF of the deeply saturated EDFA and gain dynamics can also be studied[93].

In the temporal filtering technique the signal is modulated at high speed compared with the EDFA response time. Then the amplified signal of the EDFA is chopped out and the

ASE can be thus measured at the signal wavelength. The modulation can be done using an acousto-optic modulator[89] or a mechanical chopper[V].

In the measurement system described in publication V, a single fast mechanical chopper is used for both signal modulation and temporal filtering of the ASE. Using an accurately designed chopper blade with 1/2 on/off ratio it is possible to arrange the two optical beams to be chopped so, that there are no time slots when the two channels are simultaneously on. This prevents totally the cross-talk problem between the signal and ASE. The input signal is generated using a tunable fiber ring laser, where the wavelength selection is done using the same tunable filter used in the measurement set-up, Fig. 11.

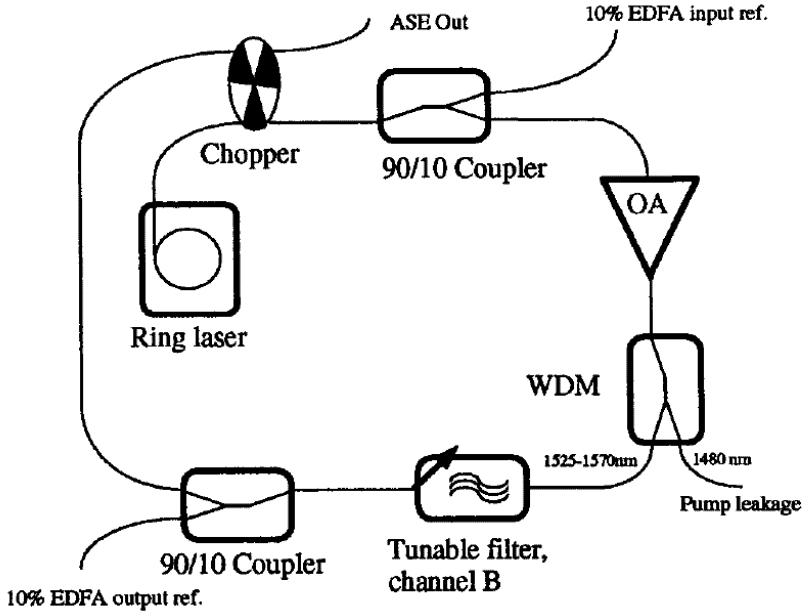

Fig. 11. The ring laser and the ASE noise power measurement unit with the optical amplifier (OA) under test[V]. The chopper cuts out the amplified signal from the ASE out fiber. Channel A of the tunable filter defines the output wavelength of the ring laser.

In analogue systems the linearity of the gain and the NF are the most important parameters of the EDFA. The chirping of the transmitter induces distortion to the signal when passed through components having wavelength dependence (gain or loss). The signal to noise ratio (SNR) and the related carrier to noise ratio (CNR) of the community antenna television (CATV) system influence directly the quality of transmission. The gain-slope can be measured using two tunable sources, one for saturating and the other for probing the gain[94]. Due to the high SNR of the CATV systems the signal power is often more than 50 dB over the ASE and thus the NF can be measured most reliably using temporal filtering[V], or by measuring the SNR degradation in the electrical domain[76,95].

3.2 Broadband EDFA

The EDFA fits well with WDM technology due to its low multichannel cross talk and broadband amplification. The reason for the low cross talk is mainly due to the long fluorescence lifetime[96] and the broad band amplification is the consequence of the Stark splitting[38]. The host glass modifies strongly the emission line shape, and using high Al doping the intrinsic gain bandwidth can be in the order of 20 nm[20,21,56], Fig. 8. The gain bandwidth can be extended to 30 nm with less than 5% gain variation using proper filtering techniques[19]. The filter can be based on di-electric interference filters, a long period grating[97,98], a short period grating[99], curved fiber[100], a Mach-Zehnder (M-Z)

interferometer type wave-guide filter[21], or an acousto-optic filter[101,102]. The problems with the long period gratings are their temperature dependence and bending sensitivity. The short Bragg gratings may create problems because they tend to reflect part of the filtered light back to the fiber. The bent type filtering suffers from long time reliability and rather high background losses. The M-Z waveguide filter suffers from extra losses and complexity in construction. The use of acousto-optic filtering is at an early stage but it has an interesting feature. The acousto-optic filter can be tuned fast and thus it provides a dynamic aspect for spectral gain control[101,102].

The controllability of the gain flatness against input power excursions has been improved by applying a tunable attenuator between two amplifying stages of the EDFA[103].

A semiconductor optical amplifier can be used to compensate the gain tilt of the EDFA[104]. The gain tilt variation due to the change of the input power can also be managed in this scheme by controlling the drive current of the semiconductor amplifiers.

3.3 L-Band EDFA

Appending the L-band EDFA to the C-band EDFA doubles the transmission bandwidth available[69]. Due to the smaller emission and absorption cross-sections at the L-band the backward ASE at C-band accumulates. This decreases the QCE of the EDFA and also the population inversion level of the EDF[69]. This degrades the noise performance. The typical NF of L-band EDFA is 5 dB[105].

Using a double stage design in which the low gain first stage is pumped using 980 nm[105] a NF of 3.6 dB is achieved. The QCE of the double stage design can be improved by using the ASE of the first stage for pumping the second stage[106]. The ASE at 1550 band can be used also for pumping an otherwise unpumped stage of the L-band EDFA and thus improve the QCE significantly from 11.7% to 25.7%[107].

By tuning the pump wavelength slightly from the peak absorption wavelength the population inversion is decreased at the pump-launching end of the EDF. This reduces the backward ASE and improves the QCE[108]. The QCE is also improved by using an idler signal in 1550 nm region[109]. The idler signal has high gain and the 980 nm pump power is converted into 1550 nm idler, which later on excites the EDF.

3.4 Dynamic gain control

Although the EDFA doesn't produce practically any crosstalk between the different wavelength channels due to the long excited state lifetime[96], there exists a rather high transient response in EDFAs to channel add / drop loss[110]. The change in the gain of EDFA can easily exceed 6 dB for the surviving channel, which is not tolerable for other parts of the network[110]. Furthermore, if there are several cascaded amplifiers in the link their combined effects disrupt the system performance via non-linearity and degradation in SNR even more[111,112].

By applying optical feedback at one wavelength it is possible to clamp the population inversion in a homogeneously broadened gain media. This also clamps the gain at other wavelengths. This optical feedback can be realized by feeding to the input of the EDFA a portion of wavelength-filtered output, which results lasing[113], Fig. 12. The filter defines the lasing wavelength, and it is not available for amplification. Linear laser structure with Bragg gratings as mirrors has also been used[114], Fig. 12.

When the input signal level of the optically gain clamped EDFA changes rapidly there is relaxation oscillation in the lasing feedback signal. This cause gain variations to the EDFA. This has to taken account in networks where several amplifiers are cascaded[45]

The benefits of the use of the linear laser structure with Bragg gratings as the optical feedback element are the simpler structure, the possibility to tune the gain by stretching one of the gratings and the minor losses at the signal wavelengths. However, the multipath interference caused by multiple reflection on the both sides of the EDF from the gratings may cause amplitude noise if the gratings have reflections at signal wavelengths[115].

Due to the lower average inversion of the L-band EDF the dynamics of the L-band EDFA are 4-5 times slower than in the C-band EDFA[116]. The all-optical gain control schemes operate also in L-band EDFAs[117].

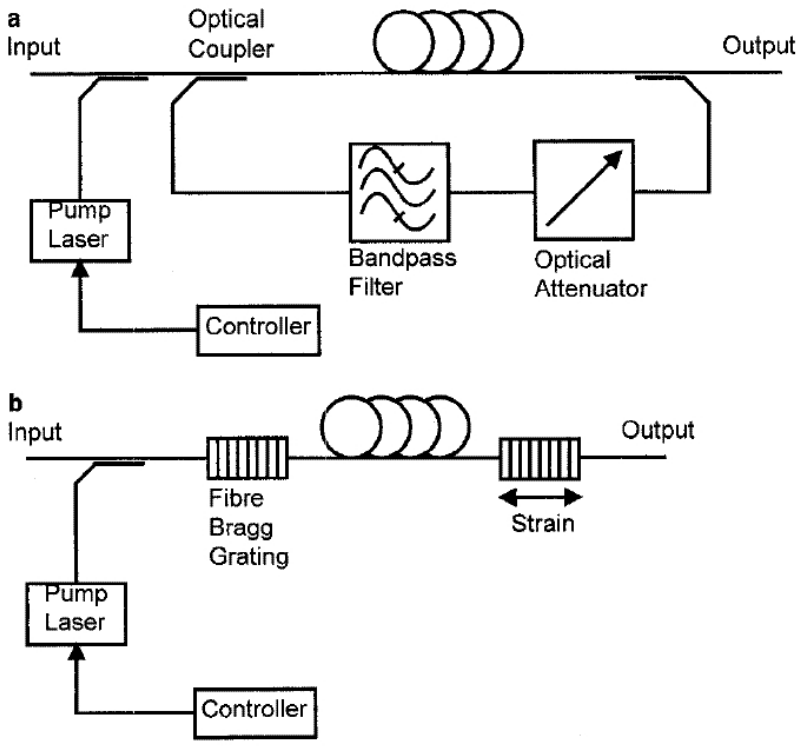

Fig. 12 The two most used all optical gain clamping configurations, a) ring laser configuration and b) fiber Bragg grating reflectors[115], © 1998 OSA.

In a fiber link it is not necessary to clamp all the EDFAs. One method is to couple the amplified feedback laser light of the first amplifier to the link[118]. The total output power of the first amplifier does not thus depend on the power of the signal channels; the lasing optical power compensates the power of the dropped signal channels. If this first gain clamped EDFA is replaced by a semiconductor optical amplifier, the compensating signal is adjusted within few nanoseconds due to the fast relaxation time of the semiconductor amplifier[119]. Due to the fast response time of the semiconductor amplifier the gain excursions of the cascaded EDFAs are almost negligible[119]. The compensating light or channel for the dropped channels can be also generated separately[120]. When the power of a single compensating channel compensates for several channels, the non-linearity in the fiber may create problems.

The assumption of homogeneously broadened gain media doesn't hold totally for EDF and thus the SHB has to be taken into account along with the relaxation oscillations of the laser when studying the dynamics of all optical gain clamped EDFAs[45]. The SHB may cause gain excursions in the order of 1 dB[121] and the gain ripples after input power change can be of the same order[45]. Especially in a fiber link with several cascaded EDFAs

these effects are multiplied. Also the gain changes become more rapid in the chain of amplifiers[111,118].

The temperature influences the population distributions in the Stark levels and there may be differences in the probabilities of the transitions between different Stark levels. This results in temperature dependence of the excited state lifetime[56] and spectral characteristics of the EDF[122]. Thus the spectral characteristics of the gain clamped amplifier are temperature dependent[122].

The other method to dynamically control the gain of EDFA is to control the pump power[123,124,VI]. A probe laser for gain measurement can be included into the EDFA to provide the pump laser control signal[123]. Also the residue pump power level can be used as the controlling signal[124]. The feed-forward scheme is also feasible; the input power level is used to control pump laser current or power[VI].

The use of a probe laser provides excellent characteristics if the speed of the electronics is fast enough. The rise time should be less than 0.5 μs to prevent ringing, which is the outcome of relaxation oscillation. The pump power loss measurement requires accurate control of the pump laser wavelength. The feed-forward control with pre-measured pump power levels requires fast digital electronics and optical components with small wavelength dependence: no other optical components are required. The electronic feed-forward control provides also the gain management for the EDFA.

4 DIRECTLY MODULATED LASER

The rather small customer base for one transmitter in the MAN and access network sets a strict cost limit for the transmitter. The directly modulated laser is the best, if not the only, solution within this cost frame. Unfortunately the fast direct modulation of laser intensity causes rapid wavelength fluctuation, chirp, in the laser output[22]. The interaction between the chirp and fiber dispersion restricts the re-generation free distance. Optimising the performance of fiber-optic communication systems requires accurate characterisation of the modulation behaviour of the transmitter. This is also essential information for the DFB laser development. For characterising the chirp of the DFB laser it is sufficient to know the variation of the centre-frequency of the single frequency laser output during modulation. The simplest way to measure it is the use of a frequency discriminator, like the solid state silicon Fabry-Perot (F-P) etalon used in this study[VII,VIII]. The solid state F-P etalon does not require repeated calibration or active stabilisation control, and the control can be done electrically enabling automatic measurements. Furthermore the silicon F-P etalon is used in this thesis for simultaneous spectral filtering and wavelength control increasing the usability of the directly modulated DFB laser[IX].

4.1 The limitations of the directly modulated laser

The modulation of the laser current alters the carrier density, which is the source for the variations in the effective refractive index. The changes in effective refractive index result in wavelength shift in the Bragg grating thus altering the laser output wavelength. In the low frequency region this variation generates adiabatic chirp, in which the wavelength variation follows the current modulation. When the modulation speed increases beyond Gb/s the transient spectral chirp starts to dominate[125]. The transient chirp originates from the relaxation oscillation between the photon and carrier density, and this causes transient fluctuations in the effective refractive index.

The chirp influences the pulse propagation in an optical fiber. Due to the transient chirp the leading and trailing edges of the pulse have slightly different carrier frequencies and, consequently, different group velocities in a dispersive fiber[22]. The combination of the frequency chirp and the chromatic dispersion of the fiber is a limiting factor for transmission spans[23,125].

The chirp of a DFB laser operating at 1.55 μm, together with the dispersion of standard SM fiber having a dispersion minimum at 1.3 μm, almost prevented earlier the use of EDFA in CATV systems. The adiabatic chirp of a typical DFB laser is in a range of 600 MHz/mA and this limits the usable analogue CATV fiber link to 10 km[126]. The use of external modulators circumvents this limitation for analogue transmission. This was possible, because in CATV system there are a large number of end-users for one transmitter. The digitalisation of CATV transmissions will make a major difference. The requirements for digitally modulated sub-carrier multiplexed systems are relaxed thus enabling the use of directly modulated DFB lasers for these CATV applications.

The introduction of integrated laser modulators and the use of external modulators have greatly reduced the limitation due to chirp, e.g., the chirp is typically around 5 Ghz when modulated with 2.5 Gbit/s[25]. Unfortunately the extra costs for the use of these rather complicated technologies restrict their utilisation.

4.2 Chirp in single frequency lasers

The intensity modulation characteristics and the frequency modulation characteristics are affected by the same fundamental material properties[22]. These properties are absorption,

gain, and refractive index dependence on carrier density. The rate equations of the single longitudinal mode laser can be written as follows[127,128]:

$$\frac{dN}{dt} = \frac{I_A}{qV_{act}} - \frac{N}{\tau_n} - g_0\left(N - N_{0g}\right)\frac{1}{\left(1+\varepsilon S\right)}S \tag{22}$$

$$\frac{dS}{dt} = \left[\Gamma g_0\left(N - N_{0g}\right)\frac{1}{\left(1+\varepsilon S\right)} - \frac{1}{\tau_p}\right]S + \Gamma\beta\frac{N}{\tau_n} \tag{23}$$

$$\frac{d\phi}{dt} = \frac{1}{2}\alpha\left[\Gamma g_0\left(N - N_{0g}\right) - \frac{1}{\tau_p}\right] \tag{24}$$

Here:

N = The electron density
S = The photon density
Γ = The optical confinement factor given by the ratio between the active gain region and the modal volume
g_0 = The gain slope constant
N_{0g} = The electron density at which the total net gain is zero
τ_p = The photon lifetime
τ_n = The electron lifetime
β = The fraction of the spontaneous emission coupled into the laser mode
V_{act} = The volume of the active layer, q is the electron charge
ε = The gain compression
I_A = The current injected into the active layer
ϕ = The optical phase
α = The linewidth enhancement

The linewidth enhancement factor α is the ratio between the change of the real part and the imaginary part of the refractive index due to the change in electron density.

Equations (22) and (23) form a relaxation oscillator between the electron density and the photon density. This oscillation is damped by spontaneous emission coupled to laser mode, gain compression via SHB and diffusion. Usually the SHB is the main damping factor[127]. This oscillation generates ringing in the output of the laser when the driving current is modulated fast.

The output power per facet is:

$$P = \frac{SV_{act}\eta h\nu}{2\Gamma\tau_p}, \tag{25}$$

here η is the quantum efficiency of the laser and h is Planck's constant. The optical frequency chirp $\Delta\nu$ is the time derivative of the optical phase[26],

$$\Delta\upsilon = \frac{1}{2\pi}\frac{d\phi}{dt}. \tag{26}$$

The large signal dynamic response of the laser is quite complex and thus necessitates numerical solution techniques[127]. The local photon densities have to also be taken into account, especially when DFB lasers are considered[128].

The chirp can be related directly to photon density S or output power P without reference to drive current by combining equations (23), (24), (25) and (26)[127],

$$\Delta\upsilon = \frac{\alpha}{4\pi}\left[\frac{d}{dt}\ln P(t) + \kappa P(t)\right], \tag{27}$$

here $\kappa = 2\Gamma\varepsilon/V_{act}\,\eta h\nu$. The first term is constant in "on" and "off" levels. During the fast turn on / off transients the chirp may be high and usually oscillates after transients due to ringing[127]. The second term describes the adiabatic chirp, where the frequency follows directly the output power. The effect of the damping on the relaxation oscillation through the gain compression ε is shown in Fig. 13

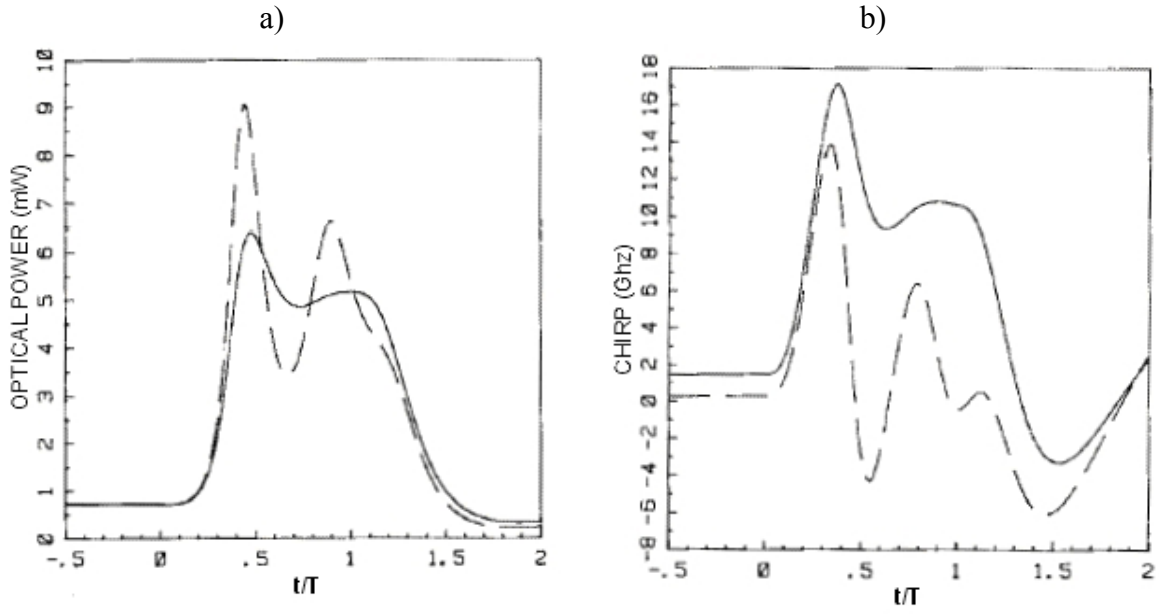

Fig. 13 Simulated a) laser output pulse and b) chirp with two different gain compressions. - - - ε = 1• 10^{-17}cm^3 and ——ε = 7• 10^{-17}cm^3 [129], © 1989 IEEE.

The relaxation oscillation and the transient chirp can be reduced by the feedback effect of the mirror loss. The relaxation oscillation is damped when the mirror loss increases with the photon density; the increased loss in the cavity moderates the build up of the photon density. The mirror loss behaviour depends on the phase shift value used between the two Bragg grating mirrors of the laser. When the phase shift is below λ/4 the mirror loss increases with photon density. The phase shift of λ/8 provides a clear improvement to the damping of the relaxation oscillation, which can be seen as reduced BER penalties[125].

The parasitics of the laser driver electronics influence current modulation and thus also the output intensity and frequency modulation. Part of the parasitics come from the package: bond wire inductance and capacitance between the input terminals. The other part comes from the chip: the stray capacitance and the resistance of the semiconducting material surrounding the active region. The parasitics can be considered as linear circuit elements. In general these parasitics produce a high frequency roll off intrinsic to the laser[127].

The driving electronics may also generate distortions like chirp noise. The chirp noise is generated in situations when the driving circuitry does not provide uniform biasing and the driving current goes to or below the threshold. Then the spontaneous emission noise results in chirp and turn-on timing jitter noise[130].

4.3 Simulation

When estimating the properties of an optical telecommunication system the parameters of the rate equation are extracted from measurements. The required parameters are: the laser threshold current, output power, resonance frequency, damping factor and the linewidth enhancement factor[26]. The adiabatic chirp generates the linewidth enhancement. The simulation results agree well, i.e. the difference between the simulated and the measured dispersion penalty is less than 0.3 dB[26].

The system simulations show that the extinction ratio[129], the decision time[27] and decision level[27] all have an effect on the performance of the system. The main contribution comes from the combination of chirp and fiber link dispersion. The optimum extinction ratio depends on the chirp and link dispersion. When the extinction rate is reduced the transient chirp is decreased: equation (27). Thus in long fiber links the reduced extinction ratio produces less dispersion penalty. Also the modulation format influences the dispersion penalty; a change from no return back to zero (NRZ) modulation to a return to zero (RZ) modulation reduces the dispersion penalty[131].

4.4 Chirp measurement techniques

The transient chirp of a repetitively driven light source is measured using a monochromator for slicing the pulses into different spectral components and a fast sampling detector[128,132]. This requires that the chirp is rather large (order of 10 GHz) due to the relatively low resolution of the monochromators. By using a narrow band F-P filter, the limitation from to monochromator can be pushed a bit but the response time of the filter itself limits the usable resolution[133,134].

For monochromatic, narrow-band sources, however, it is often sufficient to know the variation of the centre-frequency of the source output during the pulse.

Several different methods are used for measuring the variation of the centre frequency. All of the methods are based on transforming the laser frequency fluctuation to intensity variation. The used dispersive elements are fiber[135,136], a M-Z fiber interferometer[137,138], a birefringent fiber interferometer[139,140] an air-spaced F-P interferometer[141] and a solid state F-P etalon[VII,VIII]. The interferometers are used as frequency discriminators, in which the transmission depends in a linear manner on the variation of the laser frequency.

The standard SM fiber is also a dispersive element and it has been used in chirp measurement systems[135,136]. The fiber dispersion is well known and the measurement resembles the real situation in systems. Due to the nature of dispersion it is difficult or sometimes impossible to distinguish the type of the chirp from the distorted signal when the modulation (and chirp) is complex. For these reasons only sinusoidal signals have been used and a fairly large number of measurements using different fiber lengths are needed for accurate results[135,136]. It is possible to calculate the transient and the adiabatic chirp analytically when a single frequency signal is used[135]. When the modulation in the system is done using digital electronics it is not possible to make this measurement using the same driving electronics as used in the system. This eliminates the study on the combined effects of the electronics and laser.

When the interferometer is used as an optical frequency discriminator, it is tuned so that the signal is on the slope of an interference fringe. There the frequency fluctuation of the signal light change the transmission of the interferometer[137,138,139,140,141,VII,VIII]. When the change in transmission is evaluated, the frequency chirp of the signal can be calculated using the known characteristics of the filter. In many cases the interferometer can be tuned to two separate points on opposite slopes of an interference fringe. Then the

frequency chirp is obtained through subtraction of the transmitted signals detected at these two points.

When the unbalanced fiber M-Z is used as an optical discriminator[137,138] the operation point is tuned by stretching the fiber. The free spectral range (FSR) of the unbalanced M-Z is engineered by altering the fiber lengths. Fiber M-Z requires polarization control.

In a M-Z based on birefringent fibers[139,140], where the two arms of the M-Z are the two optical modes of the same fiber, the tuning can be accomplished by stretching or otherwise generating stresses to the fiber. Polarisation control is needed in this scheme; the interferometer requires equal excitation for both polarisation modes.

The F-P interferometer provides excellent filter characteristics as an optical discriminator. It operates in a large wavelength region, doesn't have any polarisation dependence and the spectral characteristics can be engineered[VII]. Several different methods have been used for the tuning and stabilisation such as movement using a piezo crystal[141], tilting of the cavity[134,VII] and changing the temperature of the interferometer[142,VIII].

The solid etalon used in publications VII and VIII was made of a standard silicon wafer polished on both sides. The use of a solid etalon as the frequency discriminator offers practical advantages. The solid etalon does not require repeated calibration or active stabilisation and control such as movement systems based on piezo crystals[141,VIII]. Furthermore, compared to two-beam interferometers[137,138,139,140], the frequency discrimination of the F-P etalon can be adjusted with more freedom by properly selecting the reflectivity and the free spectral range of the device. There is, however, always a trade-off between the wavelength selectivity and the time resolution of the interferometer.

Temperature tuning of the etalon is feasible due to the strong temperature dependence of the refractive index of silicon, $1.5 \cdot 10^{-4}$ 1/°K, and it is straightforward to implement, see Fig. 14. The effect of the thermal expansion of the chip is negligible in this application. The transmission of monochromatic light at 1.55 mm as a function of the temperature of the silicon chip is shown in Fig. 15. The temperature difference between the two reference points A and B is about 1.5 K, and the time needed for the transition from one point to the other is about 2 s.

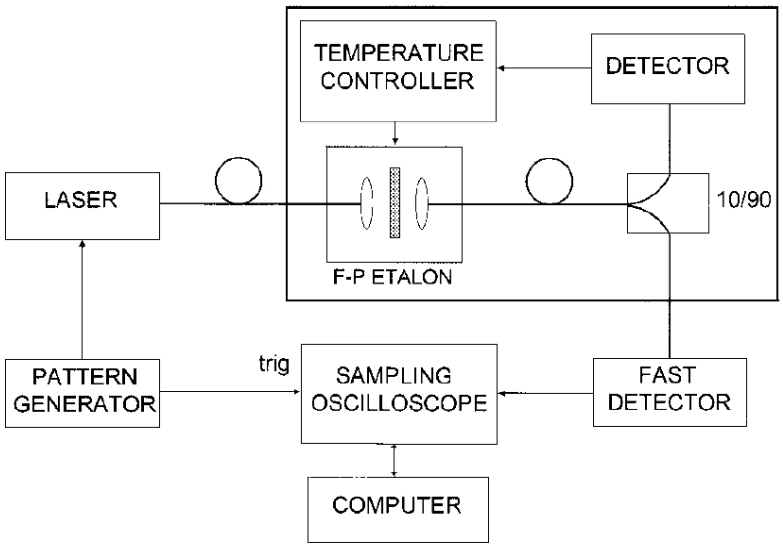

Fig. 14. The chirp measurement set up with a temperature tunable F-P interferometer[VIII].

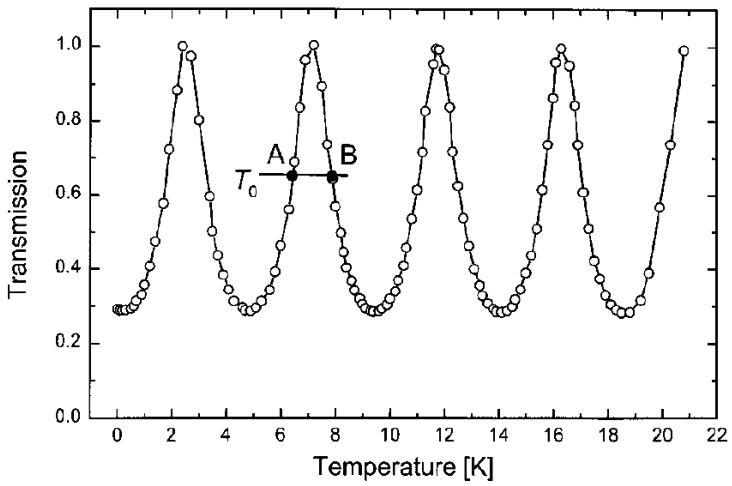

Fig. 15. The transmission of the solid silicon etalon as a function of the temperature change at 1.55 μm[VIII].

4.5 Spectral filtering

A simple method to reduce the dispersion penalty of the directly modulated DFB laser is temporal reshaping of the optical pulses by spectral filtering[28,29,30,IX], Fig. 17. The reduction on the penalty comes mainly from two effects; the extinction ratio is improved and optical power from the falling edge of the pulse is removed, Fig. 16[29,143,IX]. The improvement on the extinction ratio is due to adiabatic chirp and the sharper cut off on the falling edge of the pulse is a result of transient chirp. When the operation point of the filter is on the positive slope for example, the transmission increases with the frequency.

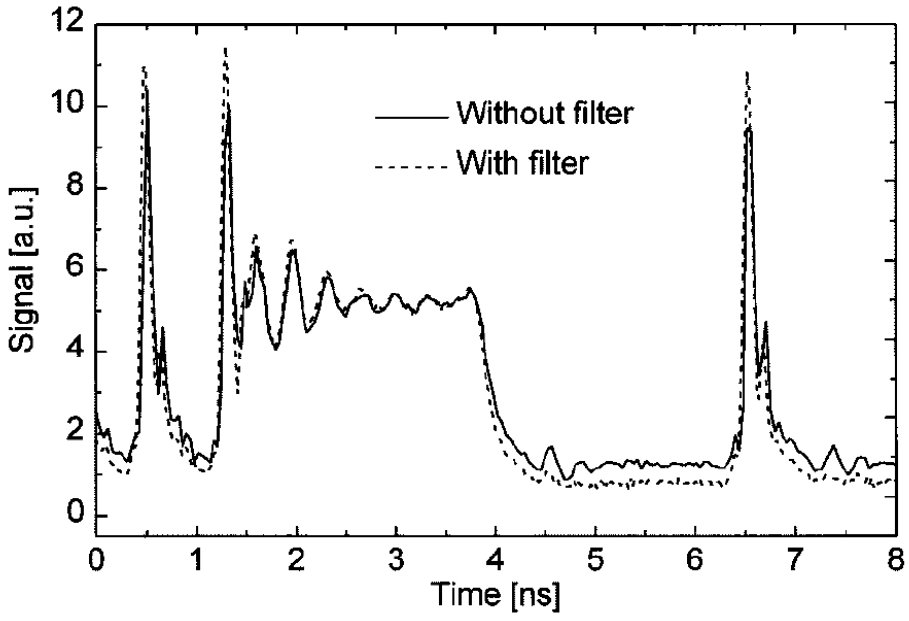

Fig. 16. The measured waveform from DFB laser signal modulated with 2.5 Gbit/s and transmitted through 350 km long fiber link with and without filtering[143], *© 2001 IEEE.*

Different types of filters have been used in these experiments: fiber F-P[29], monochromator[28], fiber Bragg grating filter[30] and silicon F-P cavity[143,IX]. All of these components have similar spectral features. The silicon F-P has excellent features, the technology is mature and the reliability of the silica material is excellent. The outcome of

these features is that the silicon F-P cavity can be used simultaneously to monitor the transmitter wavelength[IX].

The wavelength monitoring in publication IX is realised by measuring the temperature of the filter when the transmission is kept constant. The required temperature change is linearly related to the change in the laser wavelength. The temperature change was deduced from the change in the temperature sensitive thin film resistor processed on the F-P chip. The accuracy of the wavelength measurement is estimated by through a linear fit of the measured data, Fig. 18. The standard deviation of the fit is less than 2 ppm.

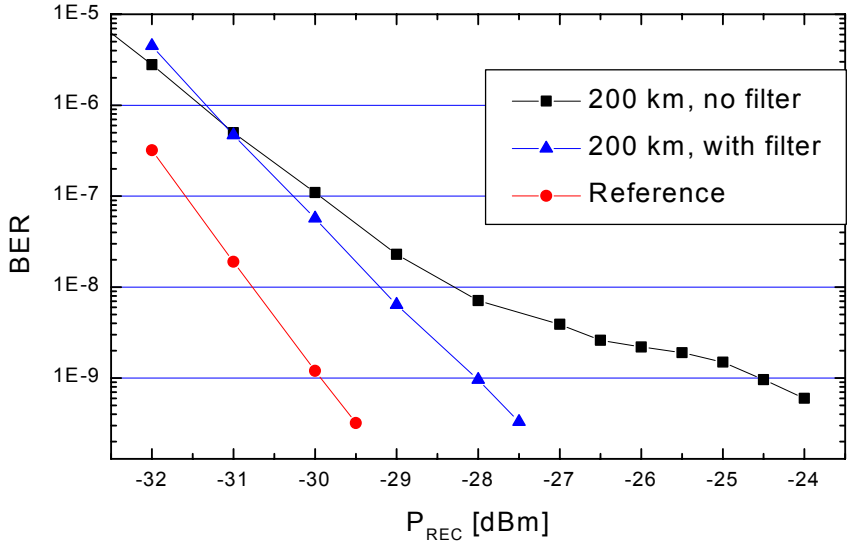

Fig. 17 The BER measurement with and without the silicon F-P filter[IX].

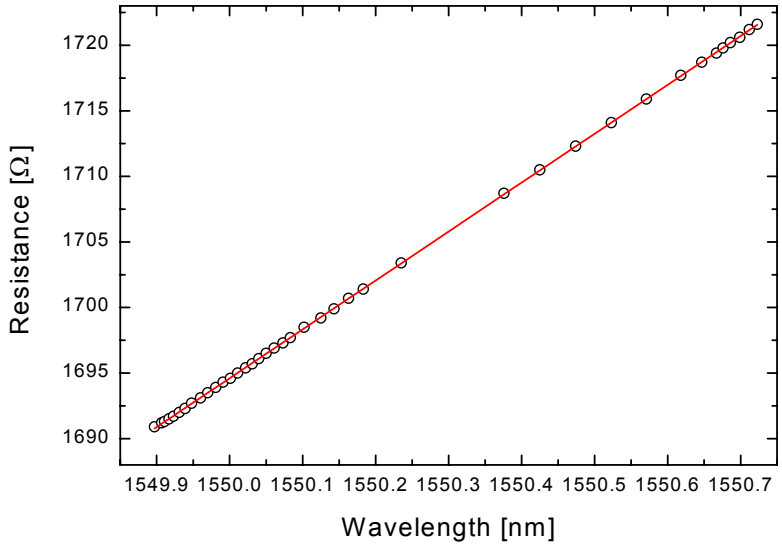

Fig. 18 Sensor resistance versus change in the wavelength of a tunable laser when feedback kept the F-P filter transmission constant[IX].

This pulse reshaping can be used also in other applications. For example, the wavelength converters based on cross gain compression in semiconductor amplifiers suffer from induced chirp[30,144] and it has been experimentally verified that spectral filtering can be used in these systems[30,145]. The pulses of the gain switched DFB lasers suffer also from chirp and their time bandwidth product can be improved significantly using F-P filters[146].

5 SDM-WDM BI-DIRECTIONAL RING NETWORK

The access networks and the routers are the bottlenecks in delivering new broadband services along with the Internet connections[1,6]. Using DWDM enables the use of the optical layer as a functional layer, which provides a new way to improve the configurability and transparency to different data protocols and signal bitrates[1,2,6,7].

The transmission needs of the feeder network require cable with several fibers[5,6]. This provides a possibility to use the SDM together with WDM. This combination offers cost reductions when compared with the heavy use of WDM with fewer fibers in the MAN[2,32,31]. A new way to organize wavelengths and fibers in optical multifiber ring network is developed and studied. The study shows that the benefits of the SDM and DWDM techniques can be combined[X].

The experimental and simulation results from this new ring network have shown that the scalability of a SDM / DWDM ring network employing bi-directional transmission[X,XI] is mainly limited by the same effects as in uni-directional ring structures when the node spacing is short[XII]. The simple node structure cuts efficiently the node cost and simultaneously decreases the optical losses remarkably. Furthermore, the number of different transmitter wavelengths used in one node is also notably reduced.

5.1 WDM ring network structures for the MANs

The MAN is more sensitive to costs than the backbone network due to the smaller customer base. This is the major limiting factor on the use of DWDM technology in the MAN[6]. Also the requirements of the access network differ remarkably from the backbone network. While the backbone network consists of point-to-point links with large and stable bandwidth needs, the access network requires finer granularity and is more agile. The access network also has to interoperate with a range of different traffic types like IP, ATM, and Gigabit Ethernet with different bitrates[6,7]. Furthermore, the price of the line terminals scales up as the square root of the transmission speed[5] thus providing lower costs per bit per km when using the long links and high bitrates with TDM instead of large number of wavelength channels with WDM.

The other main difference between the trunk network and metro networks is the link distance; in Europe the typical node spacing in the MAN is 5-15 km[9]. When the capacity is shared at the optical layer, the number of wavelengths easily becomes high. In practice this means high losses in the nodes because in most cases all the wavelengths are manipulated in the nodes. Compensation for the high node losses requires highly advanced EDFAs, which are subject to failures, need management and are expensive.

The structure of a modern high-end metro access network is pictured in Fig. 1. The network can be divided into two different parts; the distribution network and the feeder network[6,7]. The topology of the distribution network depends heavily on the needs of the customers and it can be a tree, a bus or a ring network. Also the network can be active, e.g. a legacy active SDH ring, or it can be passive depending on the bandwidth needed by the customer base in the area. The interesting feature of the WDM is that it can be used to integrate the feeder and the distribution parts of the network in a manner not available earlier. For example, the different types of services, like IP, ATM, Ethernet or legacy SDH, can be assigned to separate wavelengths. The aggregation of these diverse services can be done at the customer premises using passive optical components[7]. At the access node these wavelengths are then either tied to a particular switch selecting the type of services or are optically routed to other access nodes for switching, see Fig. 19 as an

example[6,7]. This reduces the equipment costs of the access nodes because the resources of a single switch can be shared between the other access nodes.

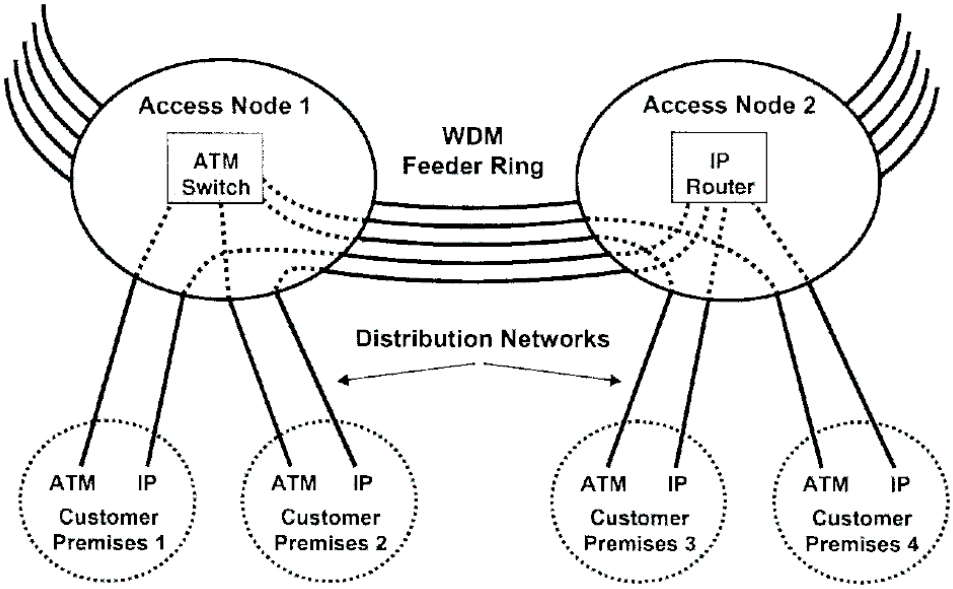

Fig. 19. In the figure an IP router is deployed in Access Node 2, but not Access Node 1. The IP traffic from Access Node 1 is routed optically directly from the distribution network of Access Node 1 to the router in Access Node 2[6], © 1999 IEEE.

The transmission needed on a high-end feeder network cable requires several fibers[2,6,7,31]. The cost effect of the multifiber cable is also relatively small compared to the installation and cabling costs[32]. This provides a possibility to use the SDM together with WDM, which will provide cost reductions when compared with the heavy use of WDM with fewer fibers in the MAN[2, 31,32,X].

The method of realizing the equipment protection is also an important cost element. In most designs several different wavelengths are used in one node. This means either doubling the line cards for protection or the use of tunable sources.

5.2 Different ring structures

WDM ring structures are well suited for metro access networks. They have in-built survivability against fiber breaks, the WDM provides the possibility for wavelength routing, and the management of a ring network is simple[6,7]. The basic WDM rings can be categorised into three basic structures: two-fiber uni-directional, four-fiber bi-directional and two-fiber bi-directional rings[5,6,31,147,148]. The protection of these architectures can be done either at the optical channel layer or at the multiplex layer. Protection at the optical channel layer means that for each trail there is also a dedicated trail for its protection. Protection at the multiplex layer means that the protection is common for all the optical channels (wavelengths) in one fiber. The protection channels can be realised by using spare fibers or spare wavelengths. By permutating all these possibilities there are twelve different ways to make basic fiber ring structures, however, some of them are not practical[5]. Two different basic two fiber ring architectures are shown with protection at the channel layer, Fig. 20, and at the multiplex layer, Fig. 21.

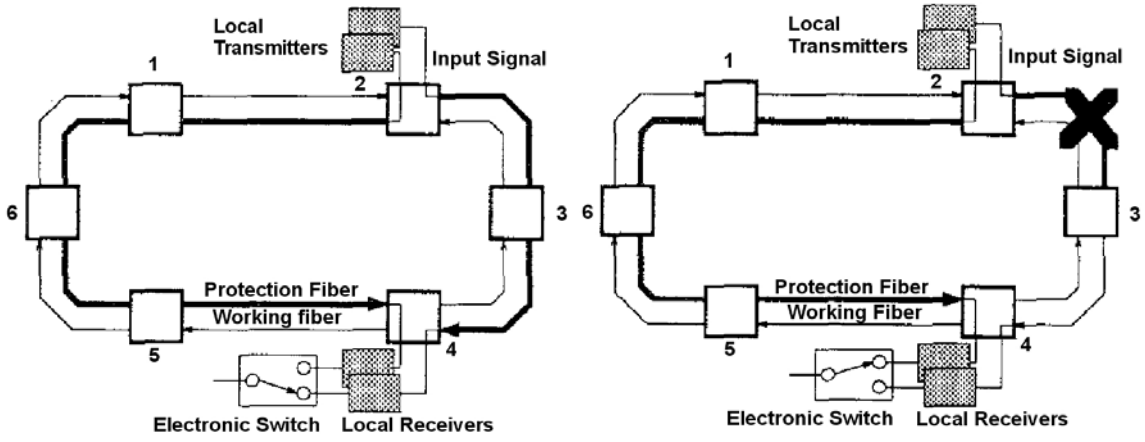

Normal scenario *Failure scenario*

Fig. 20. Schematic pictures of the two fiber uni-directional ring architecture with a spare fiber protection scheme at the channel layer (equipment layer)[148], © 1995 IEEE.

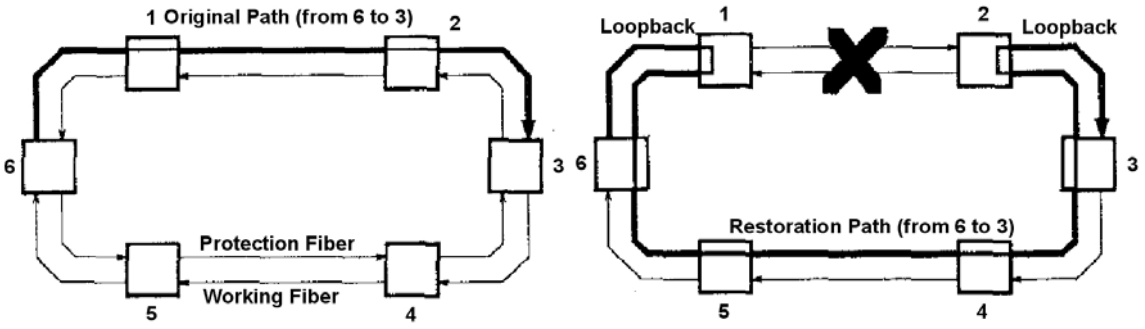

Normal scenario *Failure scenario*

Fig. 21. Schematic pictures of the two fiber uni-directional ring architectures with a spare fiber protection scheme at the optical multiplex layer[148], © 1995 IEEE.

5.3 Bi-directional transmission in one fiber

Bi-directional transmission in one fiber allows a bi-directional connection using single fiber, the allocation of the wavelength more freely, and the asymmetric bi-directional connection[X,149,150].

The amplification in a bi-directional system can be done at the multiplex layer either wavelength dependently or independently. In the wavelength dependent amplifier the direction of the amplification is defined by the wavelength[151,152,153]. This rejects the double amplification of the backscattered signal. If the amplification is done at the channel layer the amplifiers can always be uni-directional, but the number of amplifiers increases radically[149]. In the wavelength independent amplifier the amplification doesn't depend on the wavelength or the direction of the signal, which results the simplest amplifier design[XI,150]. Unfortunately the double amplified Rayleigh scattering becomes a limiting factor.

The wavelength dependent directional element is generally realised by combining one or more WDM components with optical isolators or circulators[151,152,153]. One way to realize the wavelength dependent bi-directional amplifier is to split the bi-directional signals into two spatially separated uni-directional transmission trails using circulators[152,153], Fig. 22. The two separate uni-directional amplifiers are then used for the two directions. In order to create the required wavelength selection for the passed, the added and the dropped

channels the multiplex signal is fed through an extra circulator to a DWDM component, which de-multiplexes the signal. By using fiber gratings and optical switches the passed wavelength channels are reflected back to the DWDM component, which multiplexes only the reflected channels together, and the passed multiplexed channels from the DWDM component are directed through the optical circulator to the input of the amplifier, Fig. 22. The two DWDM modules (one for each direction) used in this set-up provide also the add/drop functionality. Similar type of set-up can be built by using synchronously interleaved F-P type filter channel selection instead of expensive DWDM components, but then it is not possible to alter the directions of the wavelength channels[154].

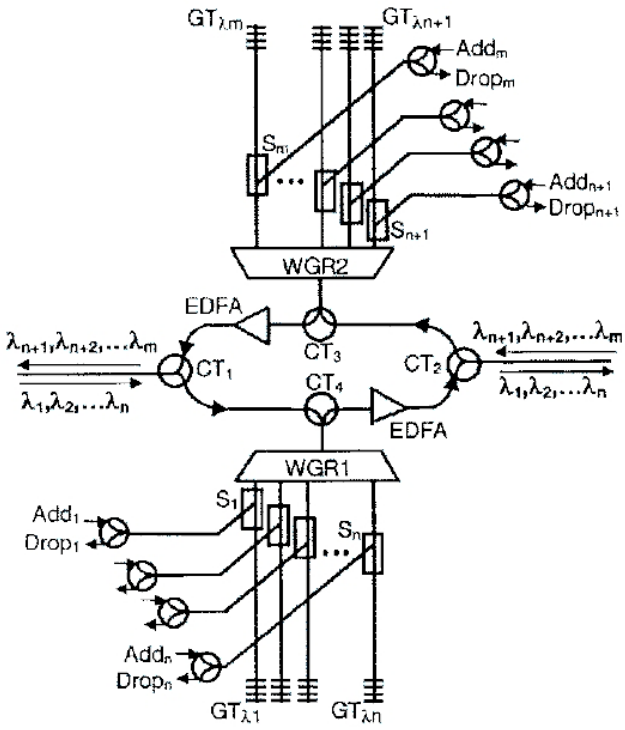

Fig. 22. Wavelength dependent bi-directional optical amplifier[153], © 1999 IEEE.

When bi-directional amplification is used, the reflected and Rayleigh backscattered light from the transmission line is doubly amplified[XI,155,156]. When the reflected and scattered signals beat with the original signal, the relative intensity noise increases due to interferometric conversion of laser phase noise to intensity noise[157,158]. This causes performance degradations to the lightwave system[159,160].

The reflections from connectors can be avoided e.g. using oblique endfaces and fusion splices but the Rayleigh backscattering of about -31 to -33 dB of the launched power cannot be avoided. The Rayleigh scattering is thus a fundamental noise source[160].

When the Rayleigh scattered signal is mixed with the original signal the generated noise spectrum is twice the original source spectral width[160]. This opens up different ways to decrease the noise. If the laser is strongly chirped, the noise spectrum is spread out from the receiver bandwidth and thus reduces the noise impact[155,160,161]. Also the use of a low coherence source like LED, F-P laser or self pulsating laser, decreases the amount of noise that falls in the bandwidth of the receiver[161]. The extra phase modulation decreases this type of noise by displacing the noise to frequencies that can be filtered out. Unfortunately this generally increases the transmitter cost notably[161].

Rayleigh scattering can be treated as a large number of mirrors having low pass filtering characteristics on the intensity modulation[162]. This simplifies the simulation, most of the

polarisation of the signal is scrambled and due to the large number of reflected beams the noise distribution is Gaussian [155].

Although Rayleigh scattering limits the use of the bi-directional wavelength independent EDFA, significant total system gain is possible as long as moderate gain for single EDFA is used[150,160,XI]. The build up of Rayleigh scattering in a bi-directional fiber link consisting of either one 20 dB gain amplifier or two 10 dB gain amplifiers is shown schematically in Fig. 23. When using one 20 dB amplifier, the Rayleigh scattered light travelling in the same direction as signal about 20 dB below signal level. By dividing the gain and the first fiber span into two parts, the aggregated Rayleigh scattering is reduced by 15 dB. The total system gain can be over 150 dB if the gain of the EDFAs are kept below the 12 dB range[160]. The bi-directional amplification has also been experimentally verified[150,XI].

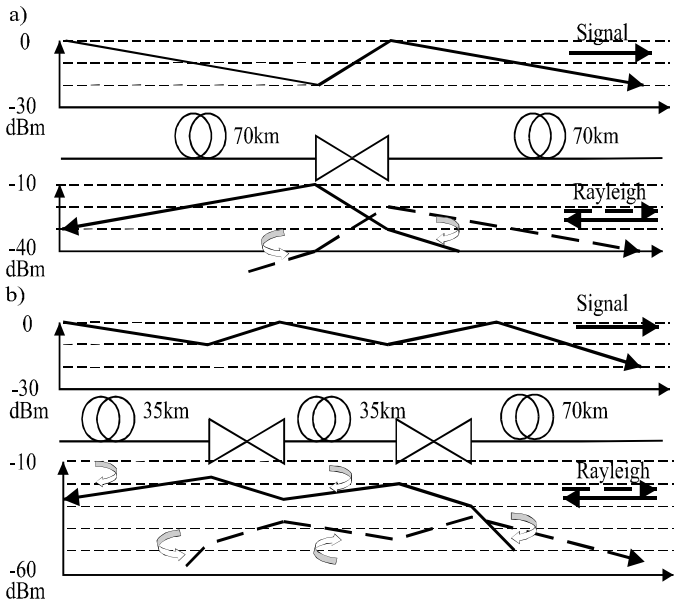

Fig. 23 The build-up of Rayleigh scattering in a fiber link a) with one 20 dB amplifier and b) with two separate 10 dB amplifiers[XI].

The Rayleigh scattered ASE power impacts also the characteristics of the bi-directional EDFA. The primary effect comes from the Rayleigh scattering of the ASE around the gain peak of the EDFA[163].

5.4 Crosstalk in WDM network

Coherent crosstalk is of concern in a WDM network node because the coherence length of a DFB laser is on the order of tens of meters[164]. It does not induce a deterministic power penalty but instead it gives rise to multipath interference and fading[162]. When the crosstalk paths are short compared with the coherence length of the laser, the statistical properties must be taken into account[164]. Then, the signal to crosstalk ratio should be greater than 40 dB for eight crosstalk paths and better than 55 dB with 32 crosstalk paths[164]. When the crosstalk paths are longer, the signal to crosstalk ratio can be lower, 35 dB for eight crosstalk paths and 45 dB for 100 paths[165]. The coherent and noncoherent crosstalk causes power penalties in practical systems and both have to be taken into account in system design. A Monte-Carlo analysis can be used to combine the effects of the two crosstalks in simulation[166].

5.5 SDM-WDM bi-directional ring network

By combining the SDM and WDM in a novel way, it is possible to reduce the number of different wavelength in one node and simultaneously cut down remarkably the optical loss for the bypassing signals[X]. When the bypass losses in the ring are low, larger networks can be achieved using less amplification.

Each node in the novel network contains one transmitter for each fiber ring, Fig. 24. The connection matrix is used to select the node to which signals are addressed. The coupling of the transmitted signals to the fiber is realised by simple, passive band-pass filters, one for each direction. This results very moderate losses for the bypassing multiplex. The band-pass WDM components also provide double isolation for the two wavelength paths operating at the same wavelength, thus preventing optical crosstalk between the two optical paths.

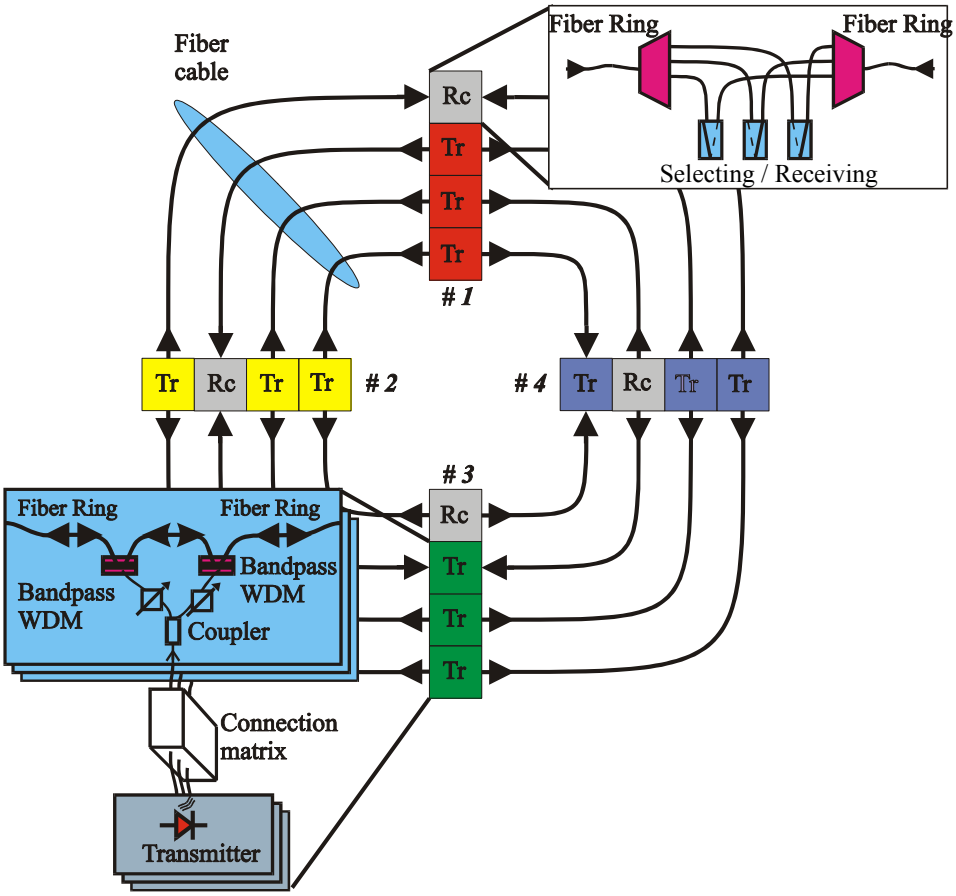

Fig. 24. The structure of the bi-directional WDM multifiber ring network with four nodes and four fibers[XI].

The fiber is terminated at its designated node where all the wavelengths are dropped and terminated, the conventional scheme in SDM[2]. Since there are two physically different wavelength paths from the transmitting node to the receiving node, the network may use either 1:1 or 1+1 protection at the optical channel or at the client layer. For example, when using 1+1 protection scheme the signal is sent both clock and anti-clockwise at the same wavelength into the same fiber ring and an optical switch at the receiving node performs the selection between the two paths. Because only one wavelength is used at one node, 1:N equipment protection can be used without tunable transmitters.

5.6 Shared-pump EDFA

Sharing of the pump laser can provide cost reductions[167,XI]. Shared-pump EDFAs with low gain can be implemented in the network, see Fig. 25. The low gain (~10-15 dB) amplifiers are used in order to prevent the scalability limitations set by the accumulating relative intensity noise (RIN) due to Rayleigh backscattering.

The use of a common pump laser and control electronics for the separate EDFAs for the different trails at the node, reduces the amplification costs remarkably in the multifiber ring. When using high pump powers compared with the relatively low output power levels of the shared-pump EDFAs, they do not require gain control.

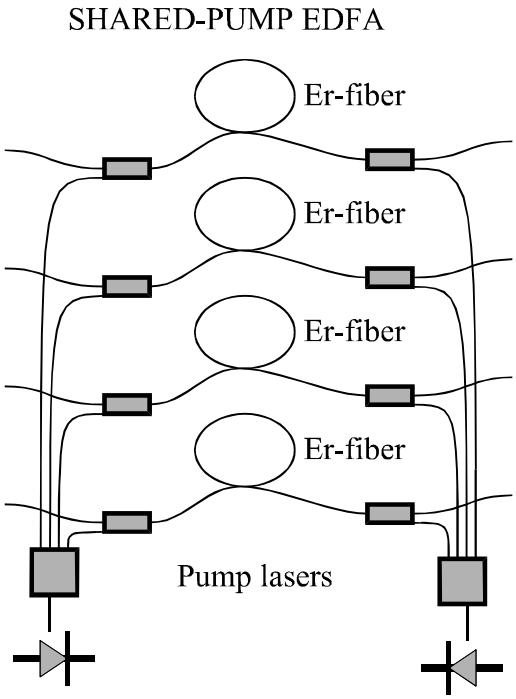

Fig. 25. The configuration of a shared-pump EDFA[XI].

5.7 Scalability

The scalability analysis is carried out by using a bi-directional transmission model for optical networks[XII] and by building a network testbed[XI]. Generally it is considered that the scalability of a bi-directional ring network is limited by the RIN arising from Rayleigh backscattering, from multiple reflections and by coherent crosstalk[164]. In practice there are, however, other limiting factors such as ASE accumulation, gain tilt, width of the gain spectrum and the input saturation power of the EDFA. The transmission model used in the scalability analysis includes: multiple Rayleigh backscattering of both signal and ASE, ASE accumulation in a cascade of bi-directional EDFAs, the gain tilt of the EDFA gain spectrum, EDFA gain dynamics, the limited width of the EDFA gain spectrum and also the simulation of optical components such as multiplexers and de-multiplexers along the signal path. The model is verified by comparing the simulation results with measurement results from an experimental network.

From the scalability simulations presented in publication XII we find out that the scalability of a metropolitan area WDM ring network employing bi-directional transmission is not mainly limited by the RIN arising from the Rayleigh backscattering. More often the gain tilt, ASE accumulation, the limited width of the gain spectrum and

EDFA's saturation power introduced more limitations. When the node spacing is 5-10 km, the main limiting factors of a bi-directional WDM multifiber ring network are the gain tilt and the input saturation power of the optical amplifier. The maximum size of the presented network is 33-43 nodes with the node spacing of 5-10 km.

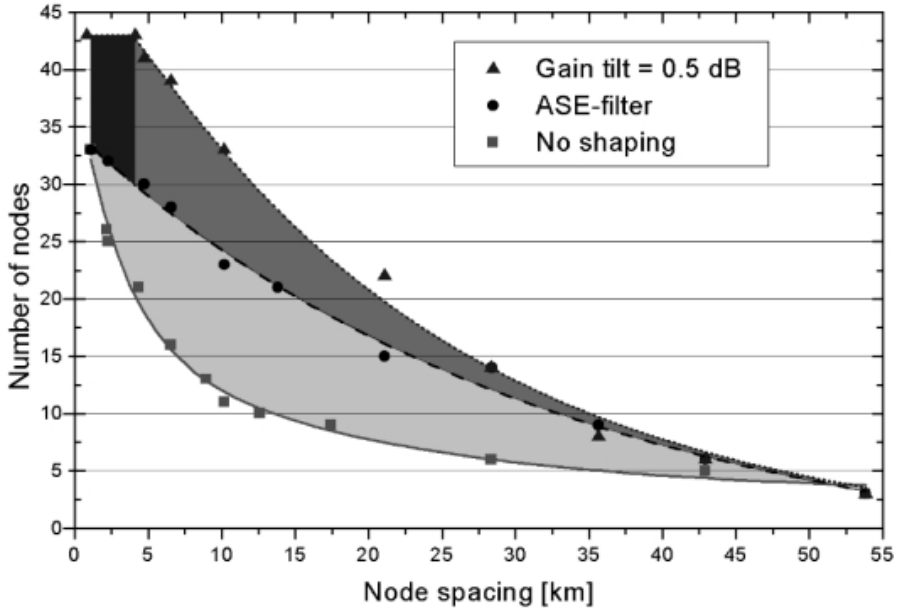

Fig. 26 Maximum size of the network with three different gain shaping schemes. $P_{in,\ sat}$= 3 dBm[168]*, © 2000 IEEE.*

6 SUMMARY AND CONCLUSION

The work presented here was carried out in a period of 13 years, covering the EDF, EDFA, the directly modulated lasers and ring metro networks. These technologies facilitated low cost broadband services for the end customer.

The EDFA was the key enabler behind present fiber-optic WDM communications. The progress of EDF started almost 20 years ago from technology that originated from the development of the transmission fibers. Due to the low vapour pressure of the rare earth halides the technology required major innovative modifications. The solution doping technique, which enabled the fabrication of the EDF, was also studied here. Although the EDF design was examined[I] and the fabrication process was improved during the course of the work[II], the doping uniformity of the glass made with this process was found to inherently limit the EDF performance. The search for a better glass fabrication process started. This lead to the development of the direct nanoparticle deposition process[17]. The DND process enabled the low cost mass production of highly doped fibers[18] with improved PMD and non-linear characteristics[III].

Studies on EDFA technology - and innovations - were accomplished alongside the progress on EDF processing technology. A new and down-to-earth technique for the accurate measurement of the NF of EDFA was developed[V]. The investigation on cladding pumping showed the benefits of the double cladding design for the high power L-band EDFA[IV]. The practical direct drive current control of the pump laser was studied in publication VI as a means of regulating and managing the gain of the EDFA. Cost effective pump laser sharing on low gain, low output power bi-directional EDFA was studied theoretically and experimentally[XI].

The wide-scale deployment of WDM in core networks and the increase of bandwidth requirements in new services in the mid-nineties awoke the interest in the use of fiber optics and WDM in the area of regional or metropolitan networks. Interest was awakened in the possibility of directly modulated sources in WDM networks because these sources could meet the strict cost requirement for the MAN. The use of solid silicon based filters resulted an accurate and stable measurement method for the critical chirp properties of directly modulated sources[VII,VIII]. As a result of further research, a component was developed for simultaneous wavelength monitoring and spectral filtering[IX]. This filter enhanced the performance of directly modulated sources in WDM networks.

The simple management and in-built protection schemes made the ring network structure the preferred choice in the MAN. A novel bi-directional WDM multifiber metropolitan ring network was proposed in the publication X. The suggested structure combined SDM and WDM in a new manner. The concept minimized the number of different wavelengths in one node and introduced minimal losses to the bypassing optical signals at the node[X]. The network concept was thoroughly developed, a demonstrator network was built, and signal transmission experiments were carried out to verify its performance[XI]. Finally an extensive scalability analysis was carried out showing that the proposed bi-directional ring network can be scaled up to a ring having more than 30 nodes and a total length of 400 km, mainly limited by the same effects as in uni-directional ring structures when the node spacing is short[XII].

REFERENCES:

[1] J. M. Simmons, A. A. M. Saleh, The value of optical bypass in reducing router size in gigabit networks, the proceedings of IEEE International Conference on Communications (ICC), **1**, 591-196, 1999.

[2] H. Obahara, H. Masuda, K. Suzuki, and K. Aida, Multifiber wavelength-division multiplexed ring network architecture for Tera-bit/s throughput, the proceedings of IEEE International Conference on Communications (ICC), 921-925, 1998.

[3] S. Bigo, Y. Frignac, G. Charlet, W. Idler, S. Borne, H. Gross, R. Dischler, W. Poehlmann, P. Tran, C. Simonneau, D. Bayart, G. Veith, A. Jourdan and J.-P. Hamaide, 10.2Tbit/s (256x42.7Gbit/s PDM/WDM) transmission over 100km TeraLight fiber with 1.28bit/s/Hz spectral efficiency, Technical Digest of the Optical Fiber Communication Conference (OFC), Post-deadline papers, PD25, 2001.

[4] B. Bakhshi, D. Kovsh, G. Mohs, R. Lynch, M. Manna, E. Golovchenko, W. Patterson, M. Vaa, P. Gorbett, M. Sanders, H. Li, G. Harvey and S. Abbott, Terabit/s field trial over the first installed dispersion-flattened transpacific system, Technical Digest of the Optical Fiber Communication Conference (OFC), Post-deadline papers, PD27-1, 2003.

[5] S. Johansson, A. Manzalini, M. Giannaccaro, R. Cadeddu, M. Giorgi, R. Clemente, R. Brändström, A. Gladisch, J. Chawki, L. Gillner, P. Öhlén, and E. Berglind, A cost-effective approach to introduce an optical WDM network in the metropolitanenvironment, IEEE Journal on Selected Areas in Communications, **16** (7), 1109-1121, 1998.

[6] A. A. Saleh and J. M. Simmons, Architectural principles of optical regional and metropolitan access networks, Journal of Lightwave Technology, **17** (12), 2431-2448, 1999.

[7] J. M. Simmons, A. A. M. Saleh, O. J. Wasem, E. A. Caridi, R. A. Barry, Optical regional access network (ORAN) project, Technical Digest of the Optical Fiber Communication Conference (OFC), **2**, 178-180, 1999.

[8] N. Chen, J. Wang, Is SDH/SONET dead?, International Optical Communication, spring, 19-21, 2003.

[9] E. Lowe, Current European WDM deployment trends, IEEE Communications Magazine, **36**(2), 46-50, 1998.

[10] K.C. Kao, G.A. Hockham, Dielectric-fiber surface waveguides for optical frequencies, Proceedings of the IEE, **113**(7), 1151-1158, 1966.

[11] F.P. Kapron, D.B. Keck, R.D. Maurer, Radiation losses in glass optical waveguides, Applied Physics Letters, **17**(10), 423-425, 1970.

[12] R. Dupuis, An introduction to the development of the semiconductor laser, IEEE Journal of Quantum Electronics, **23**(6), 651-657, 1987.

[13] C. J. Koester, E. Snitzer, Amplification in a fiber laser, Applied Optics, **3**(10), 1182-1186, 1964.

[14] S. B. Poole, D. N. Payne, M. E. Fermann, Fabrication of low-loss optical fibers containing rare-earth ions, Electronics Letters, **21**(17), 737-738, 1985.

[15] J. E. Townsend, S. B. Poole, D. N. Payne, Solution-doping technique for fabrication of rare-earth-doped optical fibers, Electronics Letters, **23**(7), 329-331, 1987.

[16] R. J Mears, L. Reekie, I. M Jauncey, D. N. Payne, Low-noise erbium-doped fibre amplifier operating at 1.54 μm, Electronics Letters, **23**(19), 1026-1028, 1987.

[17] M. Hotoleanu, P. Kiiveri, S. Tammela, S. Särkilahti, H. Valkonen, M. Rajala, J. Kurki, K. Janka, Characteristics of higly doped Er^{3+}-fibers manufactured by the new Direct Nanoparticle Deposition process, Proceedings of the 7th European Conference on Network & Optical Communications (NOC), 200-204, 2002.

[18] S. Tammela, P. Kiiveri, S. Sarkilahti, M. Hotoleanu, H. Valkonen, M. Rajala, J. Kurki, K. Janka, Direct Nanoparticle Deposition process for manufacturing very short high gain Er-doped silica glass fibers, 28th European Conference on Optical Communication (ECOC), **4**, 9.4.1-9.4.3, 2002.

[19] P. F. Wysocki, Silica-based broadband fiber amplifiers, Technical Digest of the Optical Fiber Communication Conference (OFC), Wednesday, 97-99, 1998.

[20] B. J. Ainslie, A review of the fabrication and properties of erbium-doped fibers for optical amplifiers, Journal of Lightwave Technology, **9**(2), 220-227, 1991.

[21] T. Naito, N. Shimojoh, T. Terahara, T. Tanaka, T. Chikama, M. Suyama, Long-haul WDM transmission system by use of high alumina co-doped EDFAs and gain-equalizers, The Global Telecommunications Conference (GLOBECOM), The Bridge to Global Integration, IEEE, **2**, 992 –997, 1998.

[22] T. L. Koch and J. E. Bowers, Nature of wavelength chirping in directly modulated semiconductor lasers, Electronics Letters, **20**(25/26), 1038-1039, 1984.

[23] R. A. Linke, Transient chirping in single-frequency lasers: lightwave systems consequences, Electronics Letters, **20**(11), 472-474, 1984.

[24] E.L. Wooten, K.M. Kissa, A. Yi-Yan, E.J. Murphy, D.A. Lafaw, P.F. Hallemeier, D. Maack, D.V. Attanasio, D.J. Fritz, G.J. McBrien, D.E. Bossi, A review of lithium niobate modulators for fiber-optic communications systems, IEEE Journal on Selected Topics in Quantum Electronics, **6**(1), 69-82, 2000.

[25] J. A. J. Fells, M. A. Gibbon, G. H. B. Thompson, I. H. White, R. V. Penty, A. P. Wright, R. A. Saunders, C. J. Armistead, and E. M. Kimber, Chirp and system performance of integrated laser modulators, IEEE Photonics Technology Letters, **7**(11), 1279-1281, 1995.

[26] J. C. Cartledge and R. C. Srinivasan, Extraction of DFB laser rate equation parameters for system simulation purposes, Journal of Lightwave Technology, **15**(5), 852 -860, 1997.

[27] J. C. Cartledge, and G. S. Burley, Chirping-induced waveform distortion in 2.4-Gb/s lightwave transmission systems, Journal of Lightwave Technology, **8**(5), 699-703, 1990.

[28] P. A. Morton, G. E. Shtengel, L. D. Tzeng, R. D. Yadvish, T. Tanbun-Ek, and R. A. Logan, 38.5 km error free transmission at 10 Gbit/s in standard fibre using a low chirp, spectrally filtered, directly modulated 1.55 μm DFB laser, Electronics Letters, **33**(4), 310-311, 1997.

[29] Chang-Hee Lee, Sang-Soo Lee, Hyang Kyun Kim, and Jung-Hee Han, Transmission of directly modulated 2.5-Gb/s signals over 250-km of

nondispersion-shifted fiber by using a spectral filtering method, IEEE Photonics Technology Letters, **8**(12), 1725 -1727, 1996.

[30] H. Y. Yu, D. Mahgerefteh, P. S. So, and J. Goldhar, Improved transmission of chirped signals from semiconductor optical devices by pulse reshaping using a fiber Bragg grating filter, Journal of Lightwave Technology, **17**(5), 898-903, 1999.

[31] N. Nagatsu, A. Watanabe, S. Okamoto and K. Sato, Architectural analysis of multiple fiber ring networks employing optical paths, Journal of Lightwave Technology, **15**(10), 1794-1804, 1997.

[32] J. Bannister, M. Gerla and M. Kovačević, An all optical multifiber tree network, the proceedings of INFOCOM'93, 282-292, 1993.

[33] J. Stone, C. A. Burrus, Neodymium-doped silica lasers in end-pumped fiber geometry, Applied physics Letters, **23**(7), 388-389, 1973.

[34] Stone J., Burrus C.A, Neodymium-doped fiber lasers: room temperature cw operation with an injection laser pump, Applied Optics, **13**(6), 1256-1258, 1974.

[35] S. R. Nagel, J. B. MacChesney, and K. L. Walker, Modified chemical vapor deposition. In: T. Li (editor). Optical Fiber Communications, Academic Press Inc., Orlando, Florida, 1-64, 1985.

[36] G. G. Vienne, J. E. Caplen, L. Dong, J. D. Minelly, J. Nilsson and D. N. Payne, Fabrication and characterization of Yb^{3+}:Er^{3+} phosphosilicate fibers for lasers, Journal of Lightwave Technology, **16**(11), 1990-2001, 1998.

[37] K. H. Ylä-Jarkko, Cladding pumping technology for next generation fiber amplifiers and lasers, To be presented in Optical Amplifiers and their Applications (OAA), invited paper, 2003.

[38] E. Desurvire and J. R. Simpson, Amplification of spontaneus emission in erbium-doped single-mode fibers, Journal of Lightwave Technology, **7**(5), 835-845, 1989.

[39] J. F. Marcerou, H. A.Fevrier, J. Ramos, J. C. Auge and P. Bousselet, General theoretical approach describing the complete behavior of the erbium-doped fiber amplifier, Proceeding of the conference on Fiber Laser Sources and Amplifiers II, Proc. SPIE **1373**, 168-186 1990.

[40] E. Desurvire, Erbium doped fiber amplifiers, Principles and applications, John Wiley & Sons, Inc. New York, USA, 1994.

[41] C. R. Giles, E. Desurvire, Modeling erbium-doped fiber amplifiers, Journal of Lightwave Technology, **2**, 271-283, 1991.

[42] A. Bjarklev, S. L. Hansen and J. H. Povisen, Large signal modelling of erbium doped fibre amplifier, Proceedings fo the Fiber Laser Sources and Amplifiers conference, Proc. SPIE **1171**, 118-129, 1989.

[43] N. Kagi, A. Oyobe and K. Nakamura, Gain characteristics of Er^{3+} doped fiber with a quasi-confined structure, Journal of Lightwave Technology, **8**(9), 1319-1322, 1990

[44] M. Söderlund and S. Tammela, A model of erbium-doped fiber amplifier gain dynamics, Proceedings of 18th Nordic Semiconductor Meeting, Physica Scripta, **T79**, 149-152, 1999.

[45] G. Luo, J. L. Zyskind, J. A. Nagel and M. A. Ali, Experimental and theoretical analysis of relaxation-oscillations and spectral hole burning effects in all-optical

gain-clamped EDFA's for WDM networks, Journal of Lightwave Technology, **16**(4), 527-533, 1998.

[46] T. Aizawa, T. Sakai, A. Wada, R Yamauchi, Effect of spectral-hole burning on multi-channel EDFA gain profile, Technical Digest of the Optical Fiber Communication Conference (OFC), **2**, 102-104,1999.

[47] A. A. M. Saleh, R. M. Jopson, J. D. Evankow, J. Aspell, Modeling of gain in erbium-doped fiber amplifiers, IEEE Photonics Technology Letters, **2**(10), 714-717, 1990.

[48] Y. Sun, J. L. Zyskind, A. K. Srivastava, Average inversion level, modeling, and physics of erbium-doped fiber amplifiers, IEEE Journal of selected topics in quantum electronics, **3**(4), 991–1007, 1997.

[49] S. Kai R. D. T. Lauder and M. Premaratne, Analytical model describing transients within a gain-clamped erbium-doped fiber amplifier, Technical Digest of the Optical Fiber Communication Conference (OFC), **2**, 105-107, 1999.

[50] J. Burgemeier, A. Cords, R. Marz, C. Schaffer, and B. Stummer, A black box model of EDFA's operating in WDM systems, Journal of Lightwave Technology **16** (7), 1271 -1275, 1998.

[51] R. Di Muro, S. J. Wilsson, N. E. Jolley, B. S. Farley, A. Robinson and J. Mun, A new method to determine the Er-fibre gain coefficient from dynamic gain tilt technique, Technical Digest of the Optical Fiber Communication Conference (OFC), **2**(WG3-1), 108-110, 1999.

[52] R. di Muro, The Er^{3+}-fiber gain coefficient derived from a dynamic gain tilt technique, Journal of Lightwave Technology, **18**(3), 343–347, 2000.

[53] P. Myslinski, D. Nguyen, and J. Chrostowski, Effects of Concentration on the Performance of Erbium-Doped Fiber Amplifiers, Journal of Lighwave Technology, **15(**1), 112-120, 1997.

[54] J.L. Philipsen, J. Broeng, A. Bjarklev, S. Helmfrid, D. Bremberg, B. Jaskorzynska, and B. Pálsdóttir, Observation of Strongly Nonquadratic Homogeneous Upconversion in Er -Doped Silica Fibers and Reevaluation of the Degree of Clustering, IEEE Journal of Quantum Electronics, **35(**11), 1741-1749, 1999.

[55] S. V. Sergeyev and B. Jaskorzynska, Statistical model for energy-transfer-induced up-conversion in Er^{3+}-doped glasses, Physical Review B (Condensed Matter and Materials Physics), **62**(23), 15628-15633, 2000.

[56] W. L. Barnes, R. I. Laming, E. J. Tarbox and P. R. Morkel, Absorption and emission cross section of Er^{3+} doped silica fibers, IEEE Journal of Quantum Electronics, **27**(4), 1004-1010, 1991.

[57] D.E. McCumber, Theory of Phonon-Terminated Optical Masers, Physical review, **134**(2A), A299–A306, 1964.

[58] C. Mazzali, H. L. Fragnito, E. Palange, D.C. Dini, Fast method for obtaining erbium-doped fibre intrinsic parameters, Electronics Letters, **32**(10), 921-922, 1996.

[59] B. J. Ainslie, S. P. Craig-Ryan, S. T. Davey, J. R. Armitage, C. G. Atkins, J. F. Massicot and R. Wyatt, Erbium doped fibres for efficient optical amplifiers, IEE Proceedings, **137**(4), 1990.

[60] J. Morel, A. Woodtli, R. Daniker, Characterization of the fluorescent lifetime of doped fibers by measuring the frequency transfer function, Journal of Lightwave Technology, **14**(5), 739-742, 1996.

[61] R. Wyatt, Spectroscopy of rare earth doped fibres, Proceedings of the conference Fiber Laser Sources and Amplifiers, **SPIE 1171**, 56-64, 1989.

[62] E. Desurvire, J. L. Zyskind, C. R. Giles, Design optimization for efficient erbium-doped fiber amplifiers, Journal of Lightwave Technology, **8**(11), 1730 –1741, 1990.

[63] S. Tammela, Optical mode field transformer, Finnish patent, FI85195, 1992.

[64] S. Tammela, P. Pöyhönen, and A. Tervonen, Triple Layer Refractive Index Profile for Tapered Fiber Beam Expanders, Electronics Letters, **25**(18), 1205-1206, 1989.

[65] S., Tammela, Doped mode field transforming fibre, Finnish patent, FI83708, 1991.

[66] M. N. Zervas, R. I. Laming, J. E. Townsend and D. N. Payne, Design and fabrication of high gain-efficiency erbium-doped fiber amplifiers, IEEE Photonics Technology Letters, **4**(17), 1992.

[67] M. N. Zervas, R. I. Laming and D. N. Payne, Trade-off and design considerations of the erbium-doped fibre amplifier, Digest of IEE Colloquium on Optical Amplifiers for Communications, **124**, 7/1 -7/3, 1992.

[68] B. Pedersen, M. L. Dakss, B. A. Thompson, W. J. Miniscalco, T. Wei, L. J. Andrews, Experimental and theoretical analysis of efficient erbium-doped fiber power amplifiers IEEE Photonics Technology Letters, **3**(12), 1085-1087, 1991.

[69] F. A. Flood, L-band erbium-doped fiber amplifiers, Technical Digest of the Optical Fiber Communication Conference (OFC), WG1, 2000.

[70] Y. Liu, S. Burtsev, S. Hegarty, R. Mozdy, M. Hempstead, and R. Smart, Four-wave mixing in EDFAs, Technical Digest of the Optical Fiber Communication Conference (OFC), WG4, 2000.

[71] M. Eiselt, M. Shtaif, R. W. Tkach, F. A. Flood, S. Ten, D. L. Butler, Measurements of cross-phase modulation induced crosstalk in an L-band EDFA, Technical Digest of the Optical Fiber Communication Conference (OFC), **3**, 34-36, 1999.

[72] K. Song and M. Premaratne, Effects of SPM, XPM, and Four-Wave-Mixing in L-Band EDFAs on Fiber-Optic Signal Transmission, IEEE Photonics Technology Letters, **12**(12), 2000.

[73] F. A.Flood, Impact of pump and signal wavelength on inhomogeneous characteristics of L-band EDFA's, Technical Digest of the Optical Fiber Communication Conference (OFC), WG6, 2000.

[74] P. Bousselet, M. Bettiati, L. Casca, M. Coix, F. Boubal, C. Sinet, F. Leplingard, D. Bayart, +26 dBm output power from an engineered cladding-pumped Yb-free EDFA for L-band WDM applications, Technical Digest of the Optical Fiber Communication Conference (OFC), WG5, 2000.

[75] L. Goldberg and J. Koplow, High power side-pumped Er/Yb doped fiber amplifier, Technical Digest of the Optical Fiber Communication Conference (OFC), **2**, 19-21, 1999.

[76] G. Wilson, J.-M. Delavaux, A. Stentz, I. Ryazansky, R. Windeler, M. Fishteyn and C. McIntosh, Low-noise 1-watt Er/Yb fiber amplifier for CATV distribution in HFC and FTTH/C system, Technical Digest of the Optical Fiber Communication Conference (OFC), FD1, 2000.

[77] J. P. Koplow, L. Goldberg, and D. A. V. Kliner, Compact 1-W Yb-doped double-cladding fiber amplifier using V-groove side-pumping IEEE Photonics Technology Letters, **10**(6), 793-795, 1998.

[78] F. Di Pasquale, G. Grasso, F. Meli, G. Sacchi and S. Turolla, 23 dBm output power Er/Yb co-doped fiber amplifier for WDM signals in the 1575-1605 nm wavelength region, Technical Digest of the Optical Fiber Communication Conference (OFC), **2**, 4-6, 1999.

[79] J. D. Minelly, W. L. Barnes, R. I. Laming, P. R. Morkel, J. E. Townsend, S. G. Grubb and D. N. Payne, Diode-array pumping of Er^{3+}/Yb^{3+} co-doped fiber lasers and amplifiers, IEEE Photonic Technology Letters, **5**(3), 301-303, 1993.

[80] J. M. Sousa, J. Nilsson, C. C. Renaud, J. A. Alvarez-Chavez, A. B. Grudinin, J. D. Minelly, Broad-band diode-pumped ytterbium-doped fiber amplifier with 34-dBm output power, IEEE Photonics Technology Letters, **11**(1), 39-41, 1999.

[81] M. Hofer, M. E. Fermann, L. Goldberg, High-power side-pumped passively mode-locked Er-Yb fiber laser, IEEE Photonics Technology Letters, **10**(9), 1247-1249, 1998.

[82] H. Po, E. Snitzer, R. Tumminelli, L. Zenteno, F. Hakimi, N. M. Cho and T. Haw, Double clad high brightness Nd fiber laser pumped by GaAlAs phased array, Technical Digest of the Optical Fiber Communication Conference (OFC), PD7, 1989.

[83] J. Nilsson, Cladding-pumped erbium-doped fiber amplifiers for low noise high-power WDM and analog CATV boosters-new design using ring-doping, Technical Digest of the Optical Fiber Communication Conference (OFC), 38-39, 1998.

[84] E.g., E-Tek, JDS-Uniphase or Dicon catalogues.

[85] D. J. Ripin, L. Goldberg, High efficiency side-coupling of light into optical fibres using imbedded v-grooves, Electronics Letters, **31**(25), 2204-2205, 1995.

[86] L. Goldberg, B. Cole, and E. Snitzer, V-groove side-pumped 1.5 μm fibre amplifier, Electronics Letters, **33**(25), 2127-2129, 1997.

[87] L. Goldberg, J. Koplow, Compact, side-pumped 25 dBm Er/Yb co-doped double cladding fibre amplifier, Electronics Letters, **34**(21), 2027-2028, 1998.

[88] G. Vespasiano, P. Di Cesare, M. Artiglia, T. Tambosso, Measurement of noise figure in erbium doped fiber amplifiers, Proceedings of the 8th Mediterranean Electrotechnical Conference (MELECON), **3**, 1509–1512, 13-16, 1996.

[89] Ando: Technical specifications of the Optical Amplifier Analyzer AQ8423A/B.

[90] J. Aspell, J. F. Federici, B. M. Nyman, D. L. Wilson, D. S. Shenk, Accurate noise figure measurements of erbium-doped fiber amplifiers in saturation conditions, Technical Digest of the Optical Fiber Communication Conference (OFC), ThA4, 189-190, 1992.

[91] J. F. Marecerou, H. Fevrier, J. Hervo, J. Auge, Noise characteristics of the EDFA in gain saturation regimes, in Technical Digest of Optical Amplifiers and Their Applications, OSA Technical Digest Series, **13,** ThE1, 1991.

[92] D. M. Baney and J. Dupre, Pulsed-source technique for optical amplifier noise figure measurement, 18th European Conference on Optical Communication (ECOC), WeP2.11, 509-512, 1992.

[93] K. Bertilsson, P. A. Andrekson, and B.-E. Olsson, Characterization and modelling of noise in erbium doped fiber amplifiers in the saturated regime, 19th European Conference on Optical Communication (ECOC), TuC3, 77-80, 1993.

[94] M. Artiglia, A. Pagano, M. Potenza, M. Rusconi and B. Sordo, Gain-slope measurements on erbium-doped amplifiers with different active fibers, 23rd European Conference on Optical Communication (ECOC), WE2C, paper1, 1997.

[95] S. Tammela, P. Kiiveri, K. Laine, Comparison between the measured optical noise figure and CNR degradation in an optical fibre amplifier, Symposium Record on Cable TV Sessions, 18th International television symposium and technical exhibition, 340-343, 1993.

[96] R. I. Laming, L. Reekie, P. R. Morkel, D. N. Payne, Multichannel crosstalk and pump noise characteristics of Er3+ -doped fibre amplifier pumped at 980 nm, Electronics letters, **25**(7), 455-456, 1989.

[97] P. F. Wysocki, J. B. Judkins, R. P. Espindola, M. Andrejco, A. M. Vengsarkar, Broad-band erbium-doped fiber amplifier flattened beyond 40 nm using long-period grating filter, IEEE Photonics Technology Letters, **9**(10), 1343-1345, 1997.

[98] T. Naito, T. Terahara, N. Shimojoh, T. Tanaka, T. Chikama, M. Suyama, 20-nm signal bandwidth after 147-amplifier chain using long-period gain-equalizers, Technical Digest of the Optical Fiber Communication Conference (OFC), 320-321, 1998.

[99] O. Gautheron, P. Sansonetti, G. Bassier and I. Riant, Optical gain equalisation with short period gratins, 23rd European Conference on Optical Communication (ECOC), WE2C paper 3, 1997.

[100] A.H. Llang, H. Toda, A. Maruta, A. Hasegawa, An erbium-doped fiber amplifier with dynamically gain-flattened spectrum, Technical Digest of the Optical Fiber Communication Conference (OFC), WG5, 138-139, 1998.

[101] H. S. Kim, S. H. Yun, H. K. Kim, N. Park, and B. Y. Kim, Dynamic gain equalization of erbium-doped fiber amplifier with all-fiber acousto-optic tunable filters Dynamic gain equalization of erbium-doped fiber amplifier with all-fiber acousto-optic tunable filters, Technical Digest of the Optical Fiber Communication Conference (OFC), WG5, 136-138, 1997.

[102] H. Y. Seok, W. L. Bong; K. K. Hyang and Y. K. Byoung, Dynamic erbium-doped fiber amplifier with automatic gain flattening, Technical Digest of the Optical Fiber Communication Conference (OFC), Post deadline paper, PD28-1 – PD28-3, 1999.

[103] S. Y. Park, H. K. Kim, G. Y. Lyu, H. J. Lee, J. H. Lee and S.-Y. Shin, Accurate control of output power level in gain-flattemed edfa with low noise figure, 23rd European Conference on Optical Communication (ECOC), WE1C, paper3, 1997.

[104] Ho Sung Cho; Dong Ho Lee; Hyang Kyun Kim; Sang Soo Lee, Dynamically gain-flattened hybrid optical amplifier utilizing erbium doped fiber amplifier and

semiconductor optical amplifier, 24th European Conference on Optical Communication (ECOC), **1**, 363-364, 1998.

[105] K. J. Cordina, N. E. Jolley, and J. Mun, Ultra low noise long wavelength EDFA with 3.6 dB external noise figure, Technical Digest of the Optical Fiber Communication Conference (OFC), **2**, 13-15, 1999.

[106] Seo Yeon Park, Hyang Kyun Kim, Efficient and low-noise operation in a gain-flattened 1580 nm band EDFA, Technical Digest of the Optical Fiber Communication Conference (OFC), **2**, 123-125. 1999.

[107] Ju Han Lee, Uh-Chan Ryu, Namkyoo Park, Improvement of 1.57-1.61 μm band amplification efficiency by recycling wasted backward ASE through the unpumped EDF section, Technical Digest of the Optical Fiber Communication Conference (OFC), **2**, 7-9, 1999.

[108] R. Di Muro, P. N. Kean, S. J. Wilson, and J. Mun, Dependence of L-band amplifier efficiency on pump wavelength and amplifier design, Technical Digest of the Optical Fiber Communication Conference (OFC), WG7, 2000.

[109] R. Di Muro, N. E. Jolley, and J. Mun, Measurement of the quantum efficiency of long wavelength EDFAs with and without an idler signal, 24th European Conference on Optical Communication (ECOC), 1, 419-420, 1998.

[110] A.K. Skrivastava, Y. Sun, J.L. Zyskind, J.W. Sulhoff, EDFA transient response to channel loss in WDM transmission system, IEEE Photonics Technology Letters **9**(3), pp. 386-388, 1997.

[111] Y.Sun, A.K. Srivastava, J.L. Zyskind, J.W. Sulhoff, C. Wolf and R.W. Tkach, Fast power transients in WDM optical networks with cascaded EDFAs, Electronics Letters **33**, 313-314, 1997.

[112] M. I. Hayee and A. E. Willner, Fiber transmission penalties due to EDFA power transients resulting from fiber nonlinearity and ASE noise in add/drop multiplexed WDM networks, Technical Digest of the Optical Fiber Communication Conference (OFC), **3**, ThU2-1, 307-309, 1999.

[113] M. Zirngibl, Gain control in erbium-doped fiber amplifiers by an all-optical feedback loop, Electronic Letters **27**(4), pp.560-561, 1991.

[114] J. F. Massicot, S. D. Willson, R. Wyatt, J. R. Armitage, R. Kashyap, D. Williams and R. A. Lobbett, 1480 nm pumped erbium doped fibre amplifier with all optical automatic gain control, Electronics letters, **30**(12), 962-964, 1994.

[115] N. E. Jolley, F. Davis and J. A. Mun, Bragg grating optically gain-clamped EDFA with adjustable gain, low noise figure and low multipath interference, Technical Digest of the Optical Fiber Communication Conference (OFC), 139-140, 1998.

[116] S-J. Sheih, J. W. Sulhoff, K. Kantor, Y. Sun, and A. K. Srivastava Dynamic behavior in L-band EDFA, Technical Digest of the Optical Fiber Communication Conference (OFC), WG2, 2000.

[117] M. Artiglia, A. Pagano, B. Sordo, Gain-shifted EDFA with all-optical automatic gain control, 24th European Conference on Optical Communication (ECOC), **1**, 293-294, 1998.

[118] D. H. Richards, M. A. Ali, and J. L. Jackel, A theoretical investigation of dynamic automatic gain control in multi-channel edfa cascades, 23rd European Conference on Optical Communication (ECOC), **3**, 47-50, 1997.

[119] F. Bruyere, A. Bisson, L. Noirie, J.-Y. Emery, A. Jourdan, Gain stabilization of EDFA cascade using clamped-gain SOA, Technical Digest of the Optical Fiber Communication Conference (OFC), 166 –167, 1998.

[120] J.L. Zyskind, A.K. Skrivastava, Y. Sun, J.C. Ellson, G.W. Newsome, R.W. Tkach, A.R. Chraplyvy, J.W. Sulhoff, T.A. Strasser, J.R.Pedrazzani and C. Wolf, Fast link control protection for surviving channels in multiwavelength optical networks, 22nd European Conference on Optical Communication (ECOC), **5**, 49-52, 1996.

[121] M. F. Krol, Y. Liu, J. J. Watkins and M. J. Dailey, Gain variations in optically gain clamped erbium doped fiber amplifiers 24th European Conference on Optical Communication (ECOC), **1**, 43-44, 1998.

[122] M. E. Bray and K. P. Jones, Influence of temperature and dynamic gain tilt on the choice of probe wavelength for gain control within erbium doped fibre amplifiers, 24th European Conference on Optical Communication (ECOC), **1**, 165-166, 1998.

[123] K. Motoshima, L. M. Leba, D. N. Chen, M. M. Dows, T. Li and E. Desurvire, Dynamic compensation of transient gain saturation in erbium-doped fiber amplifiers by pum feedback constrol, IEEE Photonics Technology Letters, **5**(12), 1423-1426, 1993.

[124] J. C. van der Plaats, F. W. Willems and A. M. J. Koonen, Dynamic pump-loss controlled gain-locking system for erbium-doped fiber amplifiers in multi-wavelength networks, 23rd European Conference on Optical Communication (ECOC), **3**, 127 -130, 1997.

[125] H. Yidong, K. Sato, T. Okuda, N. Suzuki, S. Ae, Y. Muroya, K. Mori, T. Sasaki, K. Kobayashi, Low-chirp and external optical feedback resistant characteristics in λ/8 phase-shifted distributed-feedback laser diodes under direct modulation, IEEE Journal of Quantum Electronics, **38**(11), 1479-1484, 2002.

[126] E. E. Bergmann, C. Y. Kuo, and S. Y. Huang, Dispersion-induced composite second-order distortion at 1.5 μm, IEEE Photonics Technology Letters, **3**(1), 59 -61, 1991.

[127] R. S. Tucker, High-speed modulation of semiconductor lasers, Journal of Lighwave Technology, **LT-3**(6), 1180-1192, 1985.

[128] J. Kinoshita, and K. Matsumoto, Transient chirping in distributed-feedback (DFB) lasers: effect of spatial hole-burning along the laser axis, IEEE Journal of Quantum electronics, **24**(11), 2160 -2169, 1988.

[129] J. C. Cartledge and G. S. Burley, The effect of laser chirping on lightwave system performance, Journal of Lightwave Technology, **7**(3), 568 -573, 1989.

[130] P. O. Andersson and K. Akermark, Generation of BER floors from laser diode chirp noise, Electronics Letters, **28**(5), 472 -474, 1992.

[131] C. R. Doerr and R. Monnard, Method for improving transmission distance of directly modulated lasers for WDM systems, 24th European Conference on Optical Communication (ECOC), **1**, 281-282, 1998.

[132] R. A. Linke, Modulation induced transient chirping in single frequency lasers, IEEE Journal of Quantum electronics, **QE-21**(6), 593-597, 1985.

[133] M. G. Davis and R. F. O'Dowd, Time-resolved spectral measurements on a multielectrode DFB laser using a Fabry–Perot interferometer, IEEE Photonics Technology Letters, **6**(1), 21–23, 1994.

[134] C. M. Olsen, H. Izadpanah, and C. Lin, Time-resolved chirp evaluations of Gbit/s NRZ and gain-switched DFB laser pulses using narrowband Fabry–Perot spectrometer, Electronics Letters, **25**(16), 1018–1019, 1989.

[135] B. W. Hakki, Dispersion of microwave-modulated optical signals, Journal of Lightwave Technology, **11**(3), 474 -480, 1993.

[136] E. Peral, W. K. Marshall, and A. Yariv, Precise measurement of semiconductor laser chirp using effect of propagation in dispersive fiber and application to simulation of transmission through fiber gratings, Journal of Lightwave Technology, **16**(10), 1874 -1880, 1998.

[137] R. A. Saunders, J. P. King, and I. Hardcastle, Wideband chirp measurement technique for high bit rate sources, Electronics Letters, **30**(16), 1336–1337, 1994.

[138] Minho Song and Shizhuo Yin, High-resolution laser chirp measurement using quadrature sampling technique, Microwave and optical technology letters, **23**(6), 335-337, 1999.

[139] R. S. Vodhanel, Frequency modulation response measurements to 15 GHz using a novel birefrigent fiber interferometer, Technical Digest of the Optical Fiber Communication Conference (OFC), **5**, 114, 1989.

[140] Y. Kotaki and H. Soda, Time-resolved chirp measurement of modulator-integrated DFB LD by using a fiber interferometer, Technical Digest of the Optical Fiber Communication Conference (OFC), **8**, 310–311, 1995.

[141] N. S. Bergano, Wavelength discriminator method for measuring dynamic chirp in DFB lasers, Electronics Letters, **24**(20), 1296–1297, 1988.

[142] T. Niemi, S. Tammela, and H. Ludvigsen, Device for frequency chirp measurements of optical transmitters in real time, Review of Scientific Instrumentation **73**(3), 1103-1107, 2002.

[143] T. Niemi, M. Uusimaa, S. Tammela, P. Heimala, T. Kajava, M. Kaivola, and H. Ludvigsen, Tunable Silicon Etalon for Simultaneous Spectral Filtering and Wavelength Monitoring of a DWDM Transmitter, IEEE Photonics Technology Letters, **13**(1), 2001.

[144] K. Inoue, Dependence of frequency chirping on bias current in LD wavelength conversion, IEEE Photonics Technology Letters, **8**(6), 767-769, 1996.

[145] K. Inoue, Optical filtering to reduce chirping influence in LD wavelength conversion, IEEE Photonics Technology Letters, **8**(6), 770-772, 1996.

[146] T. Niemi, J.-G. Zhang, and H. Ludvigsen, Effect of optical filtering on pulses generated with a gain-switched DFB laser, Optics Communications, **192**(3-6), 339-345, 2001.

[147] A. F. Elrefaie, Multiwavelength survivable ring network architectures, Conference Record on IEEE International Conference on Communications (ICC), 1245-1251, 1993.

[148] L. Wuttisittikulkij and M. J. O'Mahony, Multiwavelength self-healing ring transparent networks, IEEE Global Telecommunications Conference (GLOBECOM), **1**, 45-49, 1995.

[149] K.-P. Ho, S.-K. Liaw and C. Lin, Performance of an eight-wavelength bidirectional WDM add/drop multiplexer with 80-Gbit/s capacity, Technical

Digest of the Optical Fiber Communication Conference (OFC), TuR1, 90-91, 1997.

[150] H. Obara, H. Masuda and K. Aida, Transmission over a 200-km single-fiber bidirectional ring network with reconfigurable add/drop repeaters, 23rd European Conference on Optical Communication (ECOC), paper TH1A.3, 9-12, 1997.

[151] C.H. Kim, C.-H. Lee and Y.C. Chung, Bidirectional WDM self-healing ring network based on simple bidirectional add/drop amplifier modules, IEEE Photonics Technology Letters, **10**(9), 1340-1342, 1998.

[152] Y. Zhao, X. J. Zhao, J. H. Chen, F. S. Choa and Y. J. Chen, A novel bidirectional add/drop module for single fiber bi-directional self-healing wavelength division multiplexed ring networks, Technical Digest of the Optical Fiber Communication Conference (OFC), TuL7, 183-185, 1999.

[153] Y. Zhao, X. J. Zhao, J. H. Chen, and F. S. Choa A Novel Bidirectional Add/Drop Module Using Waveguide Grating Routers and Wavelength Channel Matched Fiber Gratings, IEEE Photonics Technology Letters, **11**(9), 1180–1182 1999.

[154] C. H. Kim and Y. C. Chung, 2.5 Gb/s 16-channel bidirectional WDM transmission system using bidirectional erbium-doped fiber amplifier based on spectrally interleaved synchronized etalon filters, IEEE Photonics Technology Letters, **11**(6), 745-747, 1999.

[155] M. J. Yadlowski and V. L. da Silva, Experimental comparison of the effect of discrete and distributed path inpand crosstalk on system performance: Application to predicting system performance penalties, Journal of Lightwave Technology, **16**(10), 1813-1821, 1998.

[156] J. L. Gimlett, M.Z. Iqbal, L. Curtis, N. K. Cheung, Impact of Multiple Reflection Noise in Gbit/s Lightwave Systems with Optical Amplifiers, Electronics Letters, **25**(20), 1393-1394, 1989.

[157] J. L. Gimlett, J. Young, R. E. Spicer and N. K. Cheung: Degradations in Gbit/s DFB Laser Transmission systems due to Phase-to-Intensity Noise Conversion by Multiple Reflection points, Electronics Letters, **24**(7), 406–408, 1988.

[158] J. L. Gimlett and N. K. Cheung: Effects of Phase to Intensity Noise Conversion by Multiple Reflections on Gigabit-per-Second DFB Laser Transmission Systems, Journal of Lightwave Technology, **7**(6), 888-895, 1989.

[159] R. K. Staubli and P. Gysel, Crosstalk penalties due to coherent Rayleigh noise in bidirectional optical communication systems, Journal of Lightwave Technology, **9**(3), 375-380, 1991.

[160] P. Wan, J. Conradi, Impact of double Rayleigh backscatter noise on digital and analog fober systems, Journal of Lightwave Technology, **14**(3), 288-297, 1996.

[161] P. J. Legg, M. Tur and I. Andonovic, Solution paths to limit interferometric noise induced performance degradation in ASK/direct detection lightwave networks, Journal of Lightwave Technology, **14**(9), 1943-1953, 1996.

[162] J. L. Gimlett, M. Z. Iqbal, N. K. Cheung, A. Righetti, F. Fontana and G. Grasso, Observation of equivalent Rayleigh scattering mirrors in lightwave systems with optical amplifiers, IEEE Photonics Technology Letters, **2**(3), 211-213, 1990.

[163] C. Delisle and J. Conradi, Model for Bidirectional Transmission in an open cascade of optical amplifiers, Journal of Lightwave Technology, **15**(5), 749-757, 1997.

[164] C. X. Yu, W.-K. Wang, and S. D. Brorson, System degradation due to multipath coherent crosstalk in WDM network nodes, Journal of Lightwave Technology, **16**(8), 1380-1386, 1998.

[165] E. L. Goldstein and L. Eskildsen, Scaling limitations in transparent optical networks to low-level crosstalk, IEEE Photonics Technology Letters, **7**(1), 93-94, 1995.

[166] S. D. Dods, J. P. R. Lacey and R. S. Tucker, Performance of WDM ring and bus networks in the presence of homodyne crosstalk, Journal of Lightwave Technology, **17**(3), 388-396, 1999.

[167] A. E. Willner, A. A. M. Saleh, H. M. Presby, D. J. DiGiovanni, and C. A. Edwards, Star couplers with gain using multiple erbium-doped fibers pumped with a single laser, IEEE Photonics Technology Letters, **3**(3), 250-252, 1991.

[168] K. Ylä-Jarkko, S. Tammela, T. Niemi, and A. Tervonen, Scalability of a Bidirectional WDM Multifiber Ring Network, 26th European Conference on Optical Communication (ECOC), Proceedings, **3**, 81-82, 2000.